AD-A074 639 MCDONNELL DOUGLAS ASTRONAUTICS CO HUNTINGTON BEACH CALIF F/G 21/2
AN ANALYSIS OF EXTERNAL BURNING PROPULSION.(U)
MAR 79 D W HARVEY F04611-78-C-0002
UNCLASSIFIED MDC-G8090 AFRPL-TR-79-8 NL

1 OF 1
AD A074639

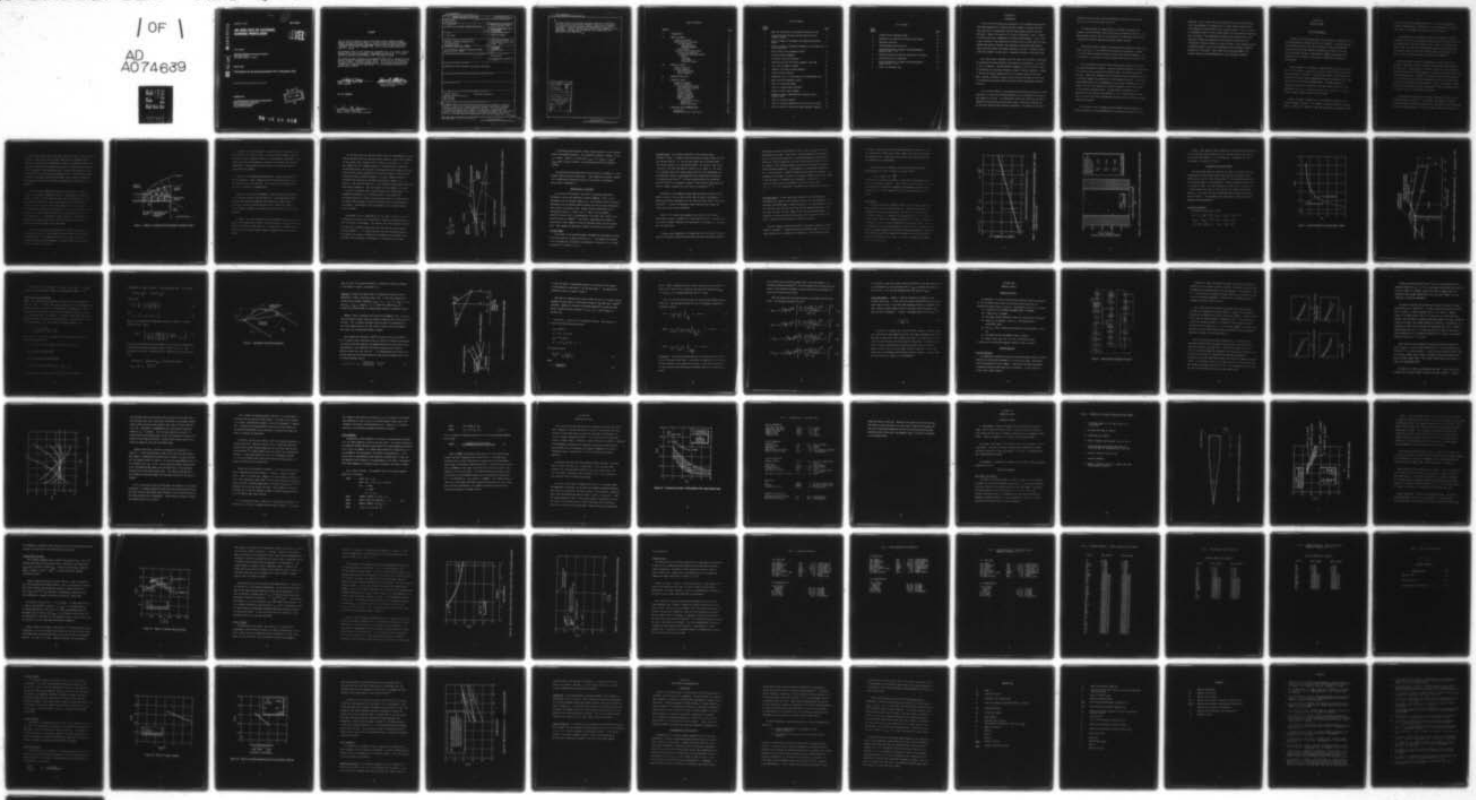

END
DATE FILMED
11-79
DDC

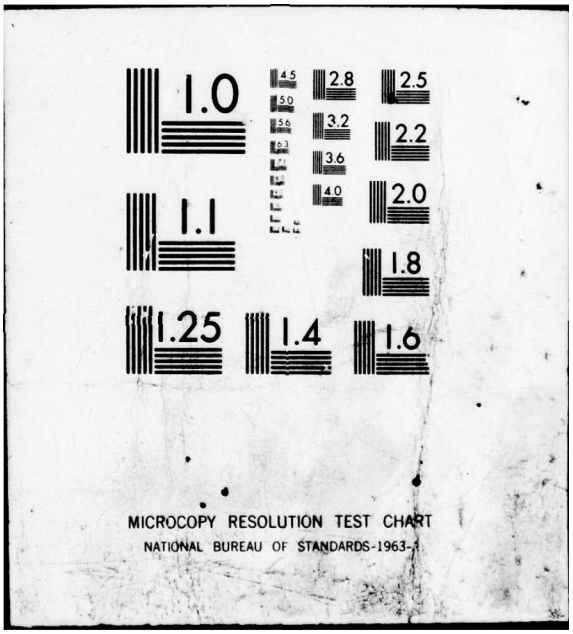
1.0
1.1
1.25
1.4
1.6
1.8
2.0
2.2
2.5
2.8
3.2
3.6
4.0
4.5
5.0
5.6
MICROCOPY RESOLUTION TEST CHART
NATIONAL BUREAU OF STANDARDS-1963-A

DDC FILE COPY AD A074639

AFRPL-TR-79-8

MDC G8090

AN ANALYSIS OF EXTERNAL BURNING PROPULSION

LEVEL II

D. W. Harvey

McDonnell Douglas Astronautics Company
5301 Bolsa Avenue
Huntington Beach, CA 92647

March 1979

Final Report for the period November 1977 to November 1978

Approved for public release: distribution unlimited

DDC
RECEIVED
OCT 4 1979
A

Prepared for

AIR FORCE ROCKET PROPULSION LABORATORY
Director of Science and Technology
Air Force Systems Command
Edwards AFB, CA 93523

79 10 03 016

FOREWORD

This is the final technical report issued under Contract F04611-78-C-0002, "External Burning Propulsion Analysis", and covers work performed by McDonnell Douglas Astronautics Company, Huntington Beach, California during the period 1 November 1977 through 1 December 1978. The Air Force project officer was Capt. R. L. Acree.

The technical effort on this program was performed by Dr. D. W. Harvey, Program Manager and Principal Investigator. Programming was done by Mr. J. C. Davis. Consulting services were provided by Prof. Ivan Catton of UCLA.

This report has been reviewed by the Information Office and is releasable to the National Technical Information Service (NTIS). At NTIS it will be available to the general public, including foreign nations. This technical report has been reviewed and is approved for publication; it is unclassified and suitable for general public release.

Robert L Acree

ROBERT L. ACREE, Capt., USAF
Project Manager

James D. Ahlstrom

JAMES D. AHLSTROM, Major, USAF
Chief, Ballistics and Space
Propulsion Branch

FOR THE COMMANDER

John H Sparks

JOHN H. SPARKS, Major, USAF
Deputy Director, Solid Rocket Division

UNCLASSIFIED

SECURITY CLASSIFICATION OF THIS PAGE *(When Data Entered)*

REPORT DOCUMENTATION PAGE

READ INSTRUCTIONS BEFORE COMPLETING FORM

1. REPORT NUMBER: AFRPL-TR-79-8	2. GOVT ACCESSION NO.
3. RECIPIENT'S CATALOG NUMBER	
4. TITLE *(and Subtitle)*: AN ANALYSIS OF EXTERNAL BURNING PROPULSION	5. TYPE OF REPORT & PERIOD COVERED: Final Technical Report, Nov 77 - Nov 78
6. PERFORMING ORG. REPORT NUMBER: MDC-G8090	
7. AUTHOR(s): D. W. Harvey	8. CONTRACT OR GRANT NUMBER(s): F04611-78-C-0002
9. PERFORMING ORGANIZATION NAME AND ADDRESS: McDonnell Douglas Astronautics Co. 5301 Bolsa Avenue Huntington Beach, CA 92647	10. PROGRAM ELEMENT, PROJECT, TASK AREA & WORK UNIT NUMBERS: Program 62302F Project 5730 Task 05 JON FA
11. CONTROLLING OFFICE NAME AND ADDRESS: Air Force Rocket Propulsion Laboratory/MKBS Edwards AFB, CA 93523	12. REPORT DATE: March 1979 13. NUMBER OF PAGES: 82
14. MONITORING AGENCY NAME & ADDRESS *(if different from Controlling Office)*	15. SECURITY CLASS. *(of this report)*: Unclassified 15a. DECLASSIFICATION/DOWNGRADING SCHEDULE

16. DISTRIBUTION STATEMENT *(of this Report)*

Approved for Public Release; Distribution Unlimited

17. DISTRIBUTION STATEMENT *(of the abstract entered in Block 20, if different from Report)*

18. SUPPLEMENTARY NOTES

19. KEY WORDS *(Continue on reverse side if necessary and identify by block number)*

External burning
External burning propulsion
Base burning
Base pressure
Supersonic combustion

20. ABSTRACT *(Continue on reverse side if necessary and identify by block number)*

A computer model of external burning propulsion of axisymmetric, supersonic vehicles is described. Reactive gaseous injectant issues from individual nozzles around the vehicle periphery, near the base. At the base these individual jets merge into an annulus of injectant surrounding the base cavity. Detailed individual-jet calculations in the region upstream of the base are made by an existing analysis developed for fuel-rich jet interaction. The

DD FORM 1 JAN 73 1473 EDITION OF 1 NOV 65 IS OBSOLETE

UNCLASSIFIED

SECURITY CLASSIFICATION OF THIS PAGE *(When Data Entered)*

389 310

injectant annulus is calculated assuming an adjustable fraction of the flow at equilibrium and the remainder frozen; mass and momentum are conserved, and the transverse pressure gradients are assumed negligible. Results and trends are presented for parameters including Mach number, altitude, vehicle geometry and injectant mass and momentum flux and composition.

Accession For
NTIS GRA&I
DDC TAB
Unannounced
Justification
By
Distribution/
Availability Codes
Dist. | Avail and/or special

TABLE OF CONTENTS

LIST OF FIGURES

LIST OF TABLES

SECTION ONE

INTRODUCTION

The use of fluid injection and combustion in the separated region behind blunt-based projectiles or vehicles has been a matter of interest for some time, ever since it became known that the base pressure could be raised by this means. Some of the early work is listed in References 1 and 2. However, as results began to be accumulated, two things became apparent. First, while a small increase in base pressure was relatively easy to obtain (and this ease implied high specific impulse), base pressures significantly above ambient values were much harder, and perhaps impossible, to reach. Second, at higher flight Mach numbers the base drag is a decreasing fraction of the total drag.

Both these factors indicated a need for higher base pressures, and methods of overcoming the ambient pressure limit began to be considered. That search is still in progress. The main method of approach is to try different means of introducing the injectant, primarily by means of lateral injection. Changes in vehicle and injector geometry and in the injectant used have also been made. However, substantial success has not yet been achieved, as can be seen by considering the two most extensive and most recent experimental programs in this area.

In the first of these[3], a strut-mounted cone-cylinder was used with lateral injection of a liquid fuel (triethylaluminum, or TEA) upstream of the base, at Mach numbers up to seven. The experimental results are classified, but may be summarized by saying that base pressures (P_B/P_∞) significantly greater than one were only obtained under transient conditions. The authors of Reference 3

conjecture that with proper design the transient results may be sustained, but this has not yet been shown to be true.

The second program of interest[4] used as injectant the exhaust of a number of solid propellants, most of which were substantially fuel-rich. Here base pressure ratios as high as 2 were obtained, but some questions of tunnel influence exist for all base pressure ratios greater than one.

These results seem to support the conclusion that substantial base pressure ratios (say $P_B/P_\infty \geq 2$) are difficult, but perhaps not impossible, to obtain. It is clear that the potential range of vehicle and injection geometries, and of injectants, is very wide, and only isolated points have been tested to date.

We are encouraged to hope for higher base pressure ratios as a result of the concept developed by Strahle[1]. Here the injectant penetrates the surrounding air stream and burns relatively far from the body, in an annulus surrounding the wake. Under these conditions the flow passing within the combustion annulus is deflected towards the centerline by a shock about the annulus. In principle rather high pressures can be generated by such a shock, especially at high Mach numbers, and such high pressures are readily transmitted to the base through the low velocity separated region. No experimental confirmation of the feasibility of this method is yet available. This is probably due at least in part to the fact that such an annular heat release region is difficult, perhaps impossible, to obtain.

At this point, then, it appears that experimental data are required to answer the question of what performance can be achieved using external burning

propulsion. But it seems likely, as illustrated by the existing data base, that high performance is available only in a very limited region of that multi-dimensional space defined by all the many variables. If this is true, an experimental search for this limited region can be prohibitively expensive, and an increase in the performance of external burning propulsion (a term used here to denote any propulsion or drag reduction scheme using the introduction of reactive fluids in or near the base) is best approached using an anlaytical model, by which the performance of many different candidate systems can be calculated. Such a model would allow experiments to be directed towards system configurations of high performance potential.

SECTION TWO

ANALYTICAL MODEL

Pre-Existing Models

A model of base burning propulsion can be developed by modifying existing base flow methods to include the effects of injection. The Crocco-Lees and Korst-Chapman approaches have been the subjects of such modification,[5, 6] but results have not been entirely satisfactory, due partly to the non-trivial problems involved in treating axial symmetry, and partly to the complexity of these methods, when regions of different fluids must be distinguished.

Another approach is to develop an analysis directly for the base burning case. This was done by Schetz et al. for base bleed only[7] and then extended to include lateral injection.[8] The model used accounts for many important features of the flow, including downstream mixing and coupling of the viscous wake flow with the inviscid surrounding flow. The model provides an interesting insight into the case of a high Mach number flow of low static temperature, but with high stagnation temperature flow there is a question whether chemical reaction heats or cools the flow.

However, the model of Schetz et al. has limitations that make it less useful for lateral injection. As it stands, it does not treat the injection process in any detail. Further, in the near wake region, it appears to treat

the cavity and the surrounding shear layer as a single one-dimensional (radially averaged) flow. Although this is a good assumption for massive base bleed, it is probably not as good for lateral injection.

The present work is an attempt to improve the treatment of lateral injection by using existing, detailed computer models of reactive liquid and gas injection (for the liquid injection case, see Ref. 9), combined into a code we refer to as BBLIP (for Base Burning/Lateral Injection Propulsion), the original version of which was produced by MDAC under contract to the Ballistic Missile Defense Advanced Technology Center (BMDATC).[10]

BBLIP calculates the flow field produced by a single transverse jet upstream of the base, and then at the base plane combines these individual jet flows into a single annulus of injectant, of which the inner boundary is the wake cavity, while the outer boundary is matched in pressure and direction to the surrounding flow. The model is entirely inviscid, but the presence of the injectant annulus avoids the indeterminacy which has long been known to exist in a single-fluid inviscid analysis; in fact, the problem is mathematically closed without requiring consideration of the reattachment pressure rise, and so this can in principle be calculated.

The individual-jet analysis was originally developed for fuel-rich jet interaction control systems[11-13]. It considers two adjacent gas streams calculated stepwise downstream, coupled by the requirement of pressure equality across the dividing steamline. The inner stream includes the jet flow plus

all the air that reacts with it; the outer stream is air only. The region near the orifice, where both streams contain large velocity components normal to the wall, is given special consideration. Mixing is treated semi-empirically, using the limited data on concentration profiles in supersonic flow appearing in the literature. Equilibrium chemistry is used to treat reaction, and any proportion of the inner flow may be assumed to react. An approximate method is used for calculating the entire flow about the jet, both for convenience and because the accuracy of the method is appropriate to other parts of the analysis.

The flow field as conceptually divided up for analysis is shown in Figure 1. The analysis proceeds as follows. Calculation of the local flow (region I) yields the state variables describing the undisturbed air stream at the point of injection. These state variables are then assumed to be uniform everywhere upstream of the shock around the jet. They are used, with the state variables of the jet, to calculate the size of the obstacle, assumed shaped like a quarter sphere, equivalent to that presented by the jet to the external flow. This calculation allows an entropy increase due to the complex shock system present in the jet, and includes the effects of jet and free stream Mach numbers and jet cant angle.

The flow of the external stream around this obstacle is obtained from the analysis of region II, which assumes inviscid compressible flow around a quarter sphere. This calculation yields both the shock shape and the pressure along the dividing streamline, the latter needed for the momentum balance in region III, to follow.

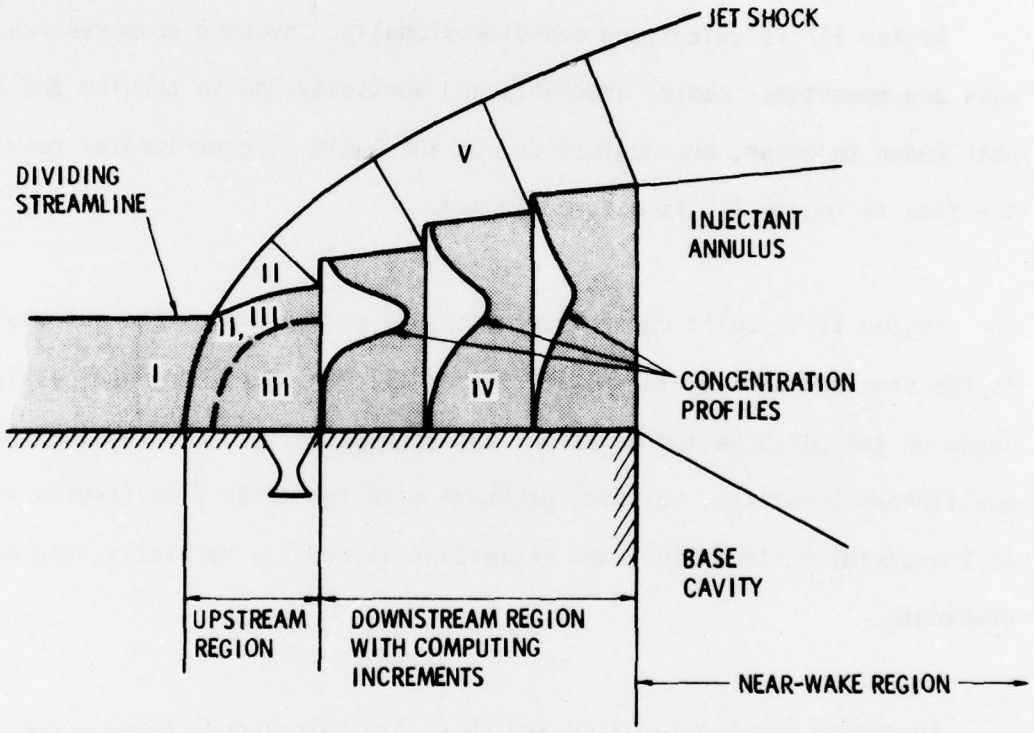

Figure 1. Model for Individual Jet Calculation Upstream of Base

In region III, a mixing analysis is used to define a point above which the fraction of jet fluid is small. This cutoff value, different values of which can be used in regions III and IV, is experimentally determined. Then, based on the flow field computed in region II, a streamline (the dividing streamline) is followed back from this point to the shock and into the undisturbed flow upstream.

Region III is calculated one-dimensionally, invoking conservation of mass and momentum. Radial gradients and vorticity due to turning the jet, both known to occur, are neglected. On the basis of experimental results, the flow in region III is assumed frozen.

Region IV is built up of increments, in each of which the calculation is the same and similar to that of region III: a one-dimensional analysis based on the conservation equations and accounting for heat release by equilibrium chemistry, matching pressure with the outer flow (region V) at the dividing streamline, and neglecting viscosity, vorticity, and normal gradients.

In region V the outer flow and shock are calculated stepwise downstream, at each step iterating with region IV on the slope of the dividing streamline, requiring pressures to match across it. The outer flow is assumed inviscid, compressible, and axially symmetric about a streamwise line in the vehicle surface.

At the base plane, the individual nozzle flows are transformed to a single annulus concentric with the body and axially symmetric, and the inner boundary of this annulus turns inward as shown in Figure 2 to an angle θ_w. In this early model, the inner boundary pressure is calculated using a simplified recirculation model, which includes a term accounting for the addition of base bleed, and thus allows evaluation of the possible synergistic effect of combining base bleed and lateral injection. The outer boundary pressure is calculated from expansion of the outer flow through an angle $\theta_c + \theta_w - \delta$, where θ_c is the cone half angle and δ is the divergence angle between inner and outer annulus boundaries. Note that because of axial symmetry, in general $\delta > 0$ even if the annulus flow is taken as frozen and without mixing. The streamwise development of the injectant annulus is calculated using equilibrium chemistry, in zones of varying concentration, to prevent losing, via cross-stream averaging, the highly nonlinear effect of concentration on heat release. Conservation of mass and momentum in the injectant annulus also is required.

Entrainment of air is accounted for via the angle σ (Figure 2), which is considered to be unknown, to be determined by comparing program predictions with the results of experiments. The external shear layer somewhat resembles the shear layer bounding a coaxial jet, for which data exist that could be used to calculate σ. It is likely, however, that the mixing half-angle of the external shear layer will depend on the geometry at the injectors where that shear layer originates, and therefore σ is preserved as an unknown.

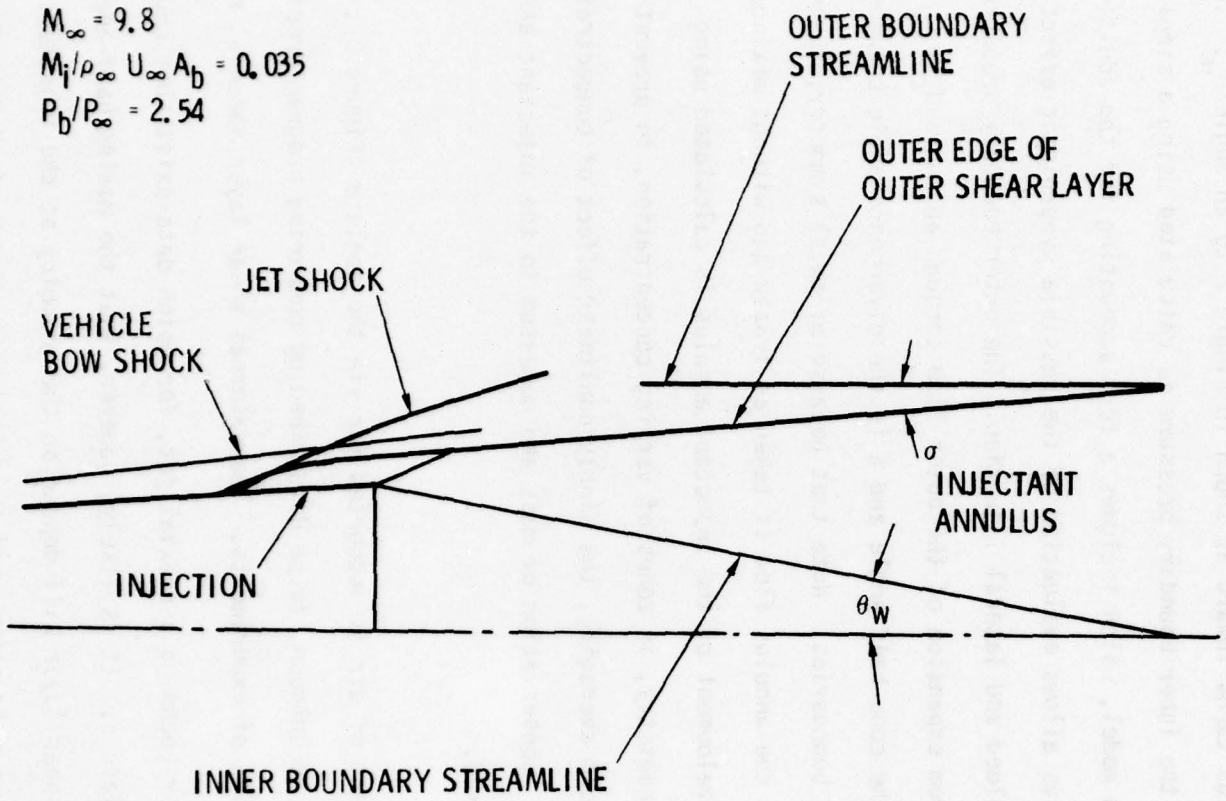

Figure 2. Injectant Annulus for Base Burning Propulsion Using Lateral Injection; Geometry Approximately to Scale

In calculating base pressure, normal pressure gradients in the injectant annulus are assumed negligible. The calculation advances as follows: First, θ_w is chosen. Second, δ is varied until $P_{exit} = 1/2\ (P_{outer} - P_{inner})/P_{outer}$ meets a preset criterion. The resulting pressure is the desired solution.

The calculations described above are also outlined in Reference 10, which contains some references to other work. A more complete description, together with an experimental program and the use of the results to determine σ, can be found in Reference 14.

Modifications to the BBLIP

At the start of the present work, BBLIP, as described above and in References 10 and 14, was deficient in several respects. First, it was developed to run at high Mach numbers only. This sufficed for the interceptor application, but the present context required the ability to run below Mach 5, down to Mach 2 and perhaps below. Second, further consideration of the reattachment process, in light of the r^{-1} terms in the axisymmetric equations of motion led to a reformulation of the model and a return to the physics observed by Chapman.[15] And finally, improvements were needed in accounting for axial symmetry in both the injectant annulus and the external flow. These changes are described in detail in the rest of this section.

Low Mach Number

At the start of the present program, individual-jet calculations upstream of the base could not be made below about $M_L = 5$. Two changes were required in the individual-jet calculation, as documented in Reference 11-13, in order to operate in the range $2 \leq M_L \leq 5$.

Upstream region: The original calculation in the upstream region (defined in Figure 1) treated inviscid flow around a quarter sphere to yield two required results: (1) the jet shock shape, and (2) pressure along the dividing streamline in the upstream region. The latter is used in the PdA term in the inner flow analysis (region III of Figure 1). The radius of the quarter sphere was a scale length called (not very accurately) the jet penetration height h, calculated from local stream and jet conditions by a method due to Kallis.[16] The flow was calculated by the approximate method of Maslen[17] as extended by Jackson;[18] the resulting shock shapes were found to compare reasonably well with high- M_L experiments.[19, 20]

Adjustments to the computer program made calculations possible at Mach numbers as low as 2.42, but this did not meet the present requirements. A method was therefore developed which uses empirical shock shapes[21] but retains the Maslen[17] - Jackson[18] integrations inward from the shock through the shock layer to the dividing streamline.

Results of this method were compared with results of the original Maslen-Jackson method, as embodied in a code known as MASJAC. The latter had been shown to compare reasonably with experiment, in the range $M_L \geq 2.42$ where both are operational.

In making these comparisons, it became clear that the values of pressure, velocity and entropy resulting from the empirical-shock calculation differed

substantially from those calculated by MASJAC, under conditions where both calculations can be made. Since MASJAC has been compared with experiment, and since the empirical expressions were developed comparing shock shapes rather than internal properties (the latter being much more sensitive than the former), it was decided to adjust the empirical expressions to match the MASJAC-calculated properties. Two parameters in the empirical expressions can be simply adjusted: standoff distance and nose radius of curvature. The importance of the former is trivial in the present context, and so only changes in the nose radius of curvature were considered. A value of R_N = 0.8 x (empirical value) gives good agreement with MASJAC over the range $2.4 < M_L < 9.8$. This expression is therefore used in BBLIP for all values of M_L.

Downstream Region: At each downstream increment in the individual-jet calculation (see Figure 1) the jet shock and inner flow are calculated. The shocklayer calculation again is done using MASJAC. At lower values of M_L, the jet shock moves away from the inner flow, and the computational rays, which are shown in Figure 1 as lines normal to the jet shock, become longer. At some point, the possibility exists that these lines may cross as the shock angle is adusted during the process of reaching a solution.

When this happens, problems can usually be avoided by choosing a smaller number of increments. A range of downstream increment number (DNI) has been found allowing runs to be made at all conditions. These results are shown

in Figure 3, which shows that for any downstream region more than 1/2 and less than about 10 scale heights long, a range of DNI exists which allows the program to run. Values too high or too low incur problems which are not theoretical but computational.

Since DNI must be an integer, the following expression, roughly corresponding to the line in Figure 3, is used in BBLIP:

$$DNI = \text{Integer} \geq 1.4 \frac{\delta z_{ds}}{h}$$

One expects DNI to affect the answer, in that mesh size generally has such an effect on numerical analysis. This effect is shown in Figure 4, in which the usual trend of reaching an asymptote with decreasing mesh size (here increasing DNI) is shown, together with the negligible magnitude of this change.

Wake Closure

It has been known since Chapman's work,[15] in 1951, that a conical base cavity cannot be truly at constant pressure. Chapman also observed, from shadowgraphs of the near wake, that the wake looks like a cone followed by a cylinder of radius R_W. Examples of this geometry can be seen in Chapman's report[15] and on page 349 of Liepmann and Roshko.[22] This shape is formed, not by streamlines, but by the outer boundary of the turbulent region. However, in supersonic flow the mixing half-angle is small (as will be discussed below), and thus the outer boundary of the turbulent region approximates a streamline. It was therefore decided to change the wake model (which up to now carried the inviscid streamlines down to $R_W = 0$, as shown in Figure 2) to require it to end at non-zero R_W.

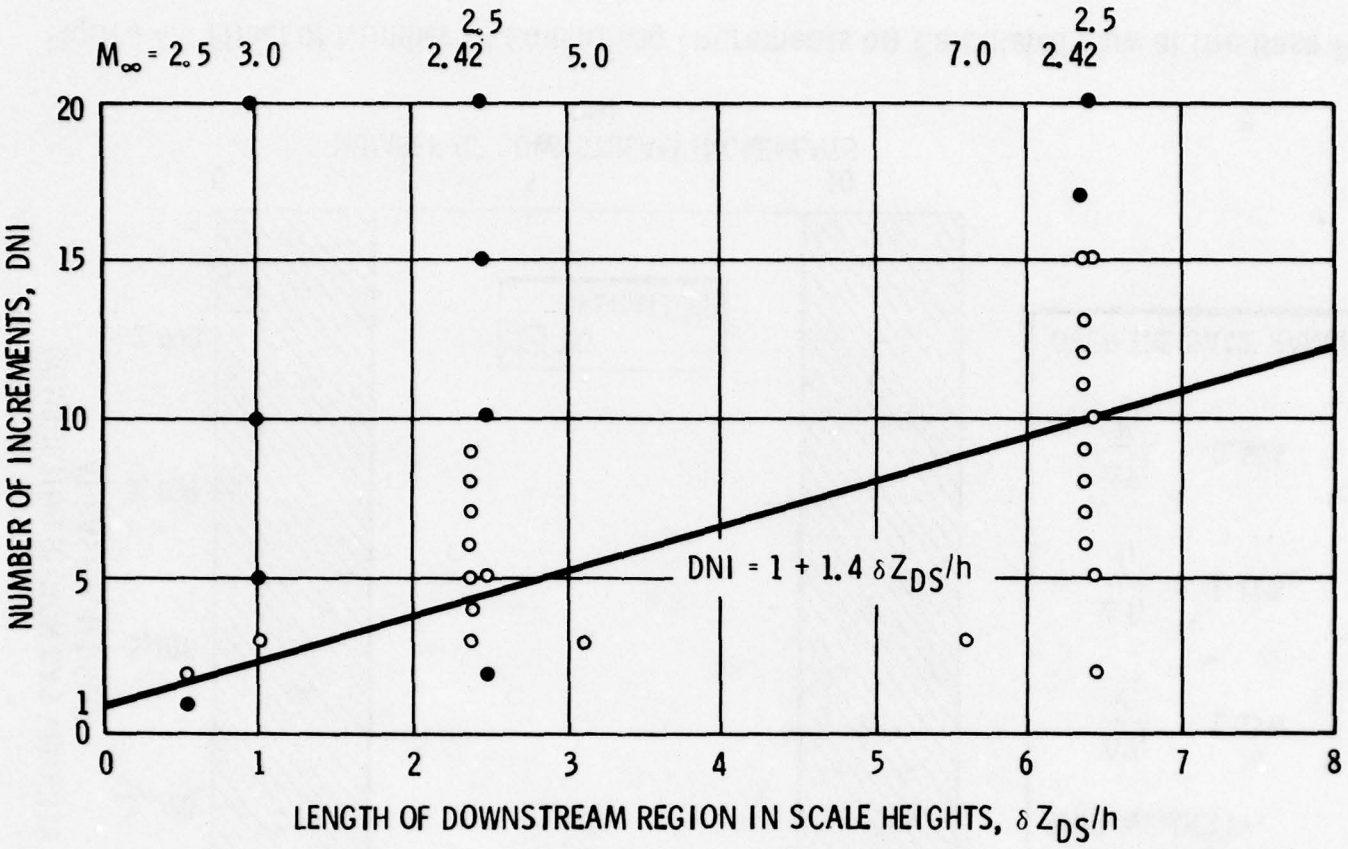

Figure 3. Choice of Number of Increments for Computing Downstream Region (Open Symbols Indicate Successful Runs)

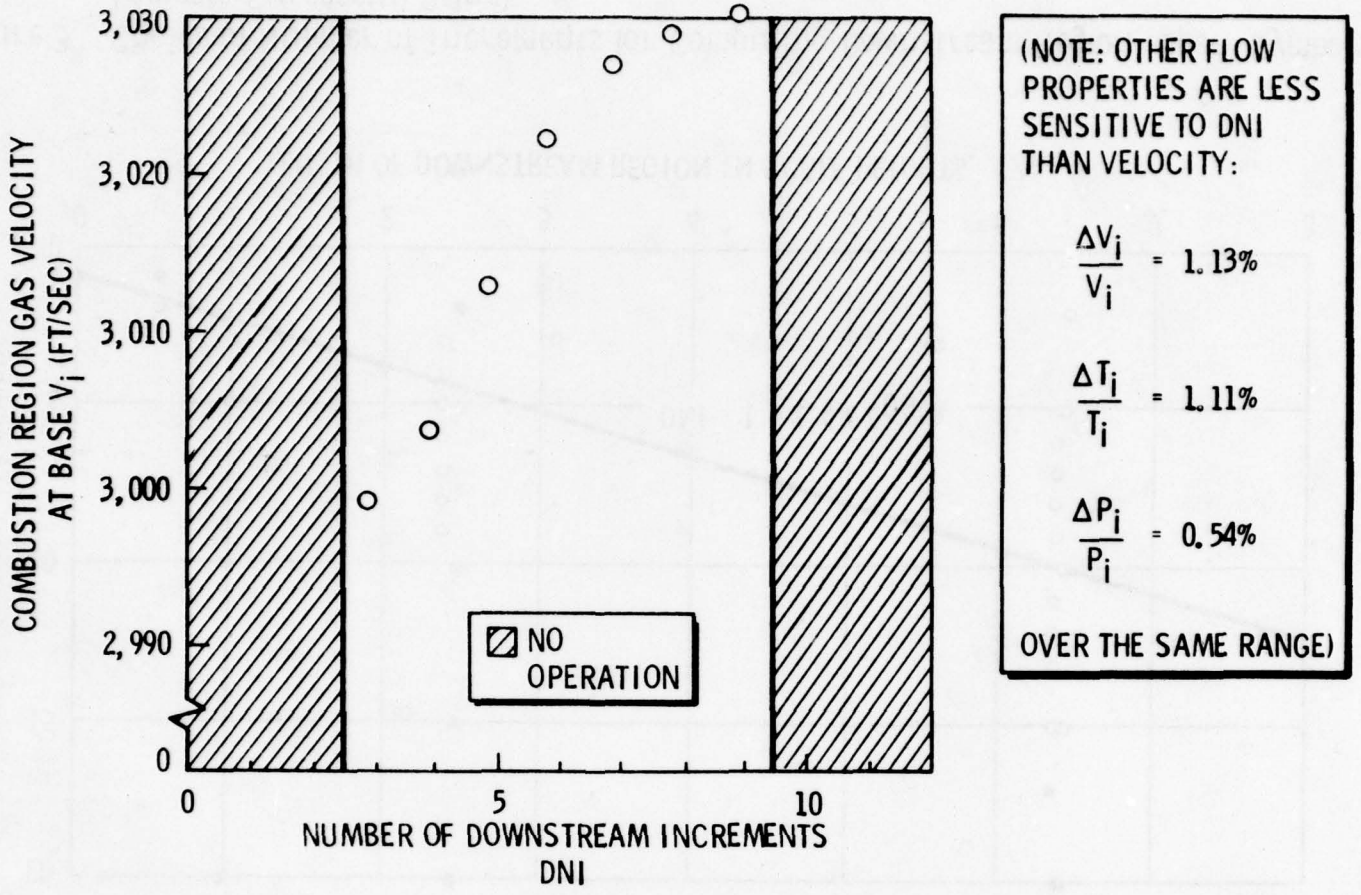

Figure 4. Effect of Number of Computing Increments on Calculated Flow at the Base Plane

Figure 5 shows Chapman's data, together with a correlation developed here. It is not entirely clear whether to use the injectant annulus Mach number m_i or the local Mach number M_L, in the correlation. Arrangements for either can be made. At present M_L is used.

Structure of the Present Model

The present model uses the individual-jet model to calculate injectant conditions at the base plane, and all these jet flows are mapped into an annulus there, just as in the previous model.[10] The downstream evolution of this injectant annulus is now calculated. Instead of making this calculation in a number of steps, as is done upstream of the base plane, a single step is taken from the base plane to the point where the annulus inner radius equals R_W. This single step uses information about the annulus geometry, as shown in Figure 6. The calculation uses conservation of mass and of axial momentum, and thermochemistry.

Conservation Equations

The conservation equations become

$$P_i A_i + P_{in}\,\pi\,(R_B^2 - R_W^2) + P_{out\,u}\,\pi\,(R_{turn}^2 - (R_B + R_1)^2)$$
$$+ P_{out\,d}\,\pi\,(R_{turn}^2 - R_3^2) + \dot{m}_i\,v_i + \delta\dot{m}_u\,v_1 + \delta\dot{m}_d\,v_2 \qquad (1)$$
$$- (\dot{m}_i + \delta\dot{m}_u + \delta\dot{m}_d)\,V_{i+1} = P_{i+1}\,\pi\,(R_3^2 - R_W^2)$$

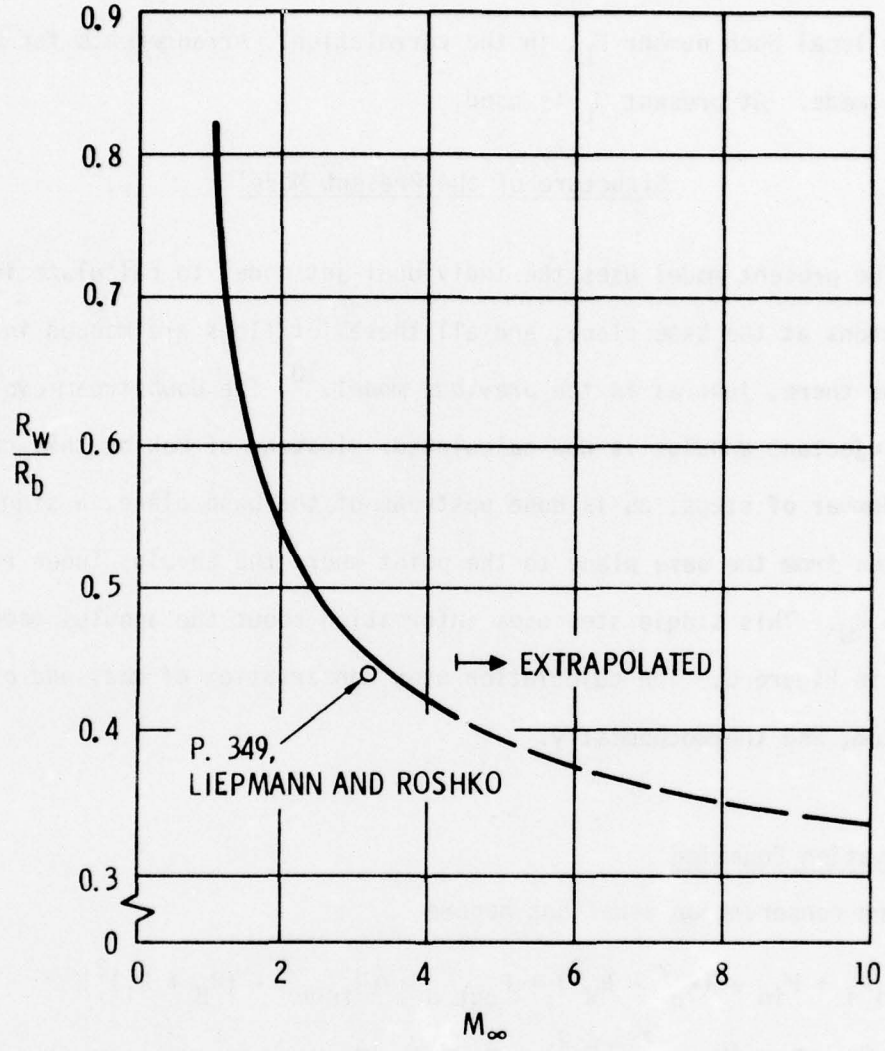

Figure 5. Wake Thickness for Axisymmetric Bodies

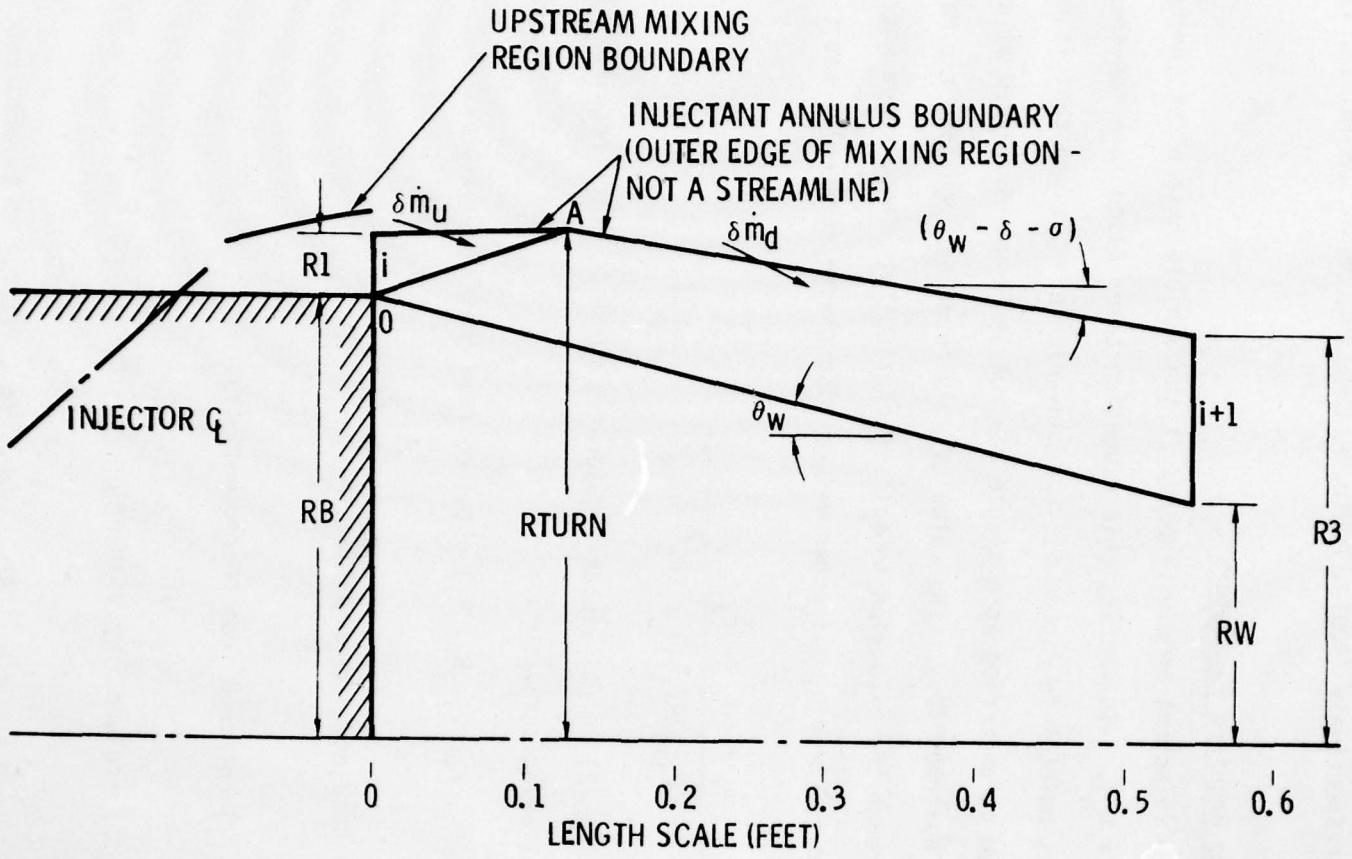

Figure 6. Injectant Annulus Geometry (Approximately to Scale for $M_\infty = 3$, $m_j/\rho_\infty V_\infty A_b = 0.0313$

Finding the latter 8 parameters is the key to the problem. In FORTRAN these are respectively (POUTU, POUTD, PIN, RTURN, DMDTU, DMDTD, V1, V2).

Finding the Required Parameters

RTURN: The injectant annulus expands at the vehicle base plane through the angle ($\theta_c = \theta_w$). In reality this expansion takes place in a fan-shaped region centered at point A in Figure 6. For convenience we assume that it can be represented as occurring at a single ray, OA in Figure 6, placed at an angle α to the upstream flow. The value of α is found by requiring the Mach number change through the expansion to satisfy continuity. Then, since the expansion is assumed isentropic, all other values also change correctly, and

$$V_{i+1} = \frac{\dot{m}_i + \delta\dot{m}_u + \delta\dot{m}_d}{(P_{i+1}/RT_{i+1})\ \pi\ (R_3^2 - R_W^2)} \qquad (2)$$

Substituting (2) in (1) yields a quadratic for R_3^2, which requires values of the following parameters:

(P_i, A_i, $\dot{m}_i$, v_i, R_B, R_1) obtained from initial conditions

(R_W) obtained from experiment[15]

(RT_{i+1}) obtained from thermochemistry

(P_{i+1}) obtained from assumption $P_{i+1} = P_{out\ d} = P_{in}$

($P_{out\ u}$, $P_{out\ d}$, P_{in}, R_{turn}, $\delta\dot{m}_u$, $\delta\dot{m}_e$, V_1, V_2) to be obtained.

The geometry is shown in Figure 7. Using continuity and $P = \rho RT$, we have

$$P_1 R_1 M_1 \sqrt{T_2} = P_2 r_2 M_2 \sqrt{T_1}$$

which yields

$$\frac{r_2}{r_1} = \frac{M_1}{M_2} \left(\frac{1 + \frac{\gamma-1}{2} M_1^2}{1 + \frac{\gamma-1}{2} M_2^2} \right) \tag{3}$$

Also

$$\sin \alpha = \frac{r_1}{L} \quad , \sin (\alpha + \theta) = \frac{r_2}{L} \tag{4}$$

where L is the length of the equivalent single ray (Figure 7). Solving (3) and (4) for α yields

$$\alpha = \tan^{-1} \left[\frac{\sin \theta}{\frac{M_1}{M_2} \left(\frac{1 + \frac{\gamma-1}{2} M_1^2}{1 + \frac{\gamma-1}{2} M_2^2} \right)^{-\frac{\gamma+1}{2(\gamma-1)}} - \cos \theta} \right] \tag{5}$$

Since we are discussing flow in the annulus, $M_1 = M_i$ and M_2 is obtained from a Prandtl-Meyer expansion through θ; Figure 6 shows $\theta = \theta_w + \theta_c$. Thus interpreted, (5) yields α from known initial conditions and an assumed value of θ_w.

From Figure 6, α determines R_{turn}. Assuming small angles,

$$R_{turn} = R_B + R_1 \frac{\theta_c + \phi + \alpha}{\alpha - \sigma} \tag{6}$$

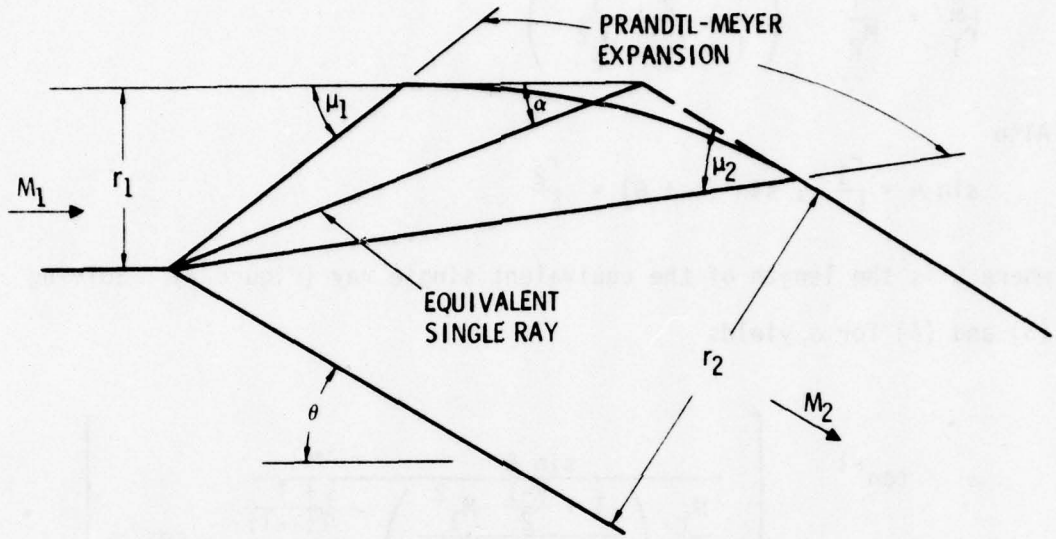

Figure 7. Equivalent Single Ray Expansion

Thus the first of the required variables is determined, based on knowledge of the angles in Figure 6, particularly Θ_w.

Pressures: Assuming the angles known, the bounding pressures are easily determined if Figure 6 describes planar flow. In that case pressures are constant along straight streamlines, $P_{out\ u} = P_i$, $P_{in} = P_i + \delta P_{PM}(\theta_c + \theta_w)$, and $P_{out\ d} = P_{out\ u} + \delta P_{PM}(\Theta_c + \Theta_w - \delta)$, where the notation $\delta P_{PM}(\theta)$ refers to the pressure drop in a Prandtl-Meyer expansion through the angle Θ.

However, Figure 6 represents not planar but axisymmetric flow. In such a flow the pressure changes along any straight streamline that is not parallel to the axis. This is readily calculated using the method of characteristics, but in the present analysis the flow field of Figure 6 must be calculated many times, and an approximate method is needed.

Such a method was developed by Webb[23] and used by Mehta and Strahle[24]. This is based on Webb's observation that the effects of streamline convergence, in a typical near-wake geometry, are communicated mainly by the right-running characteristics, the "reflected" left-running characteristics playing a relatively minor role (see Figure 8). This approximation then allows us to use the characteristic relation along the right-running characteristic, which in finite difference form is

$$\theta_3 - \theta_2 = \nu_3 - \nu_2 + \frac{\sin\theta \sin\mu_2}{\sin(\theta + \mu_2)} \frac{r_3 - r_2}{r_2} \qquad (7)$$

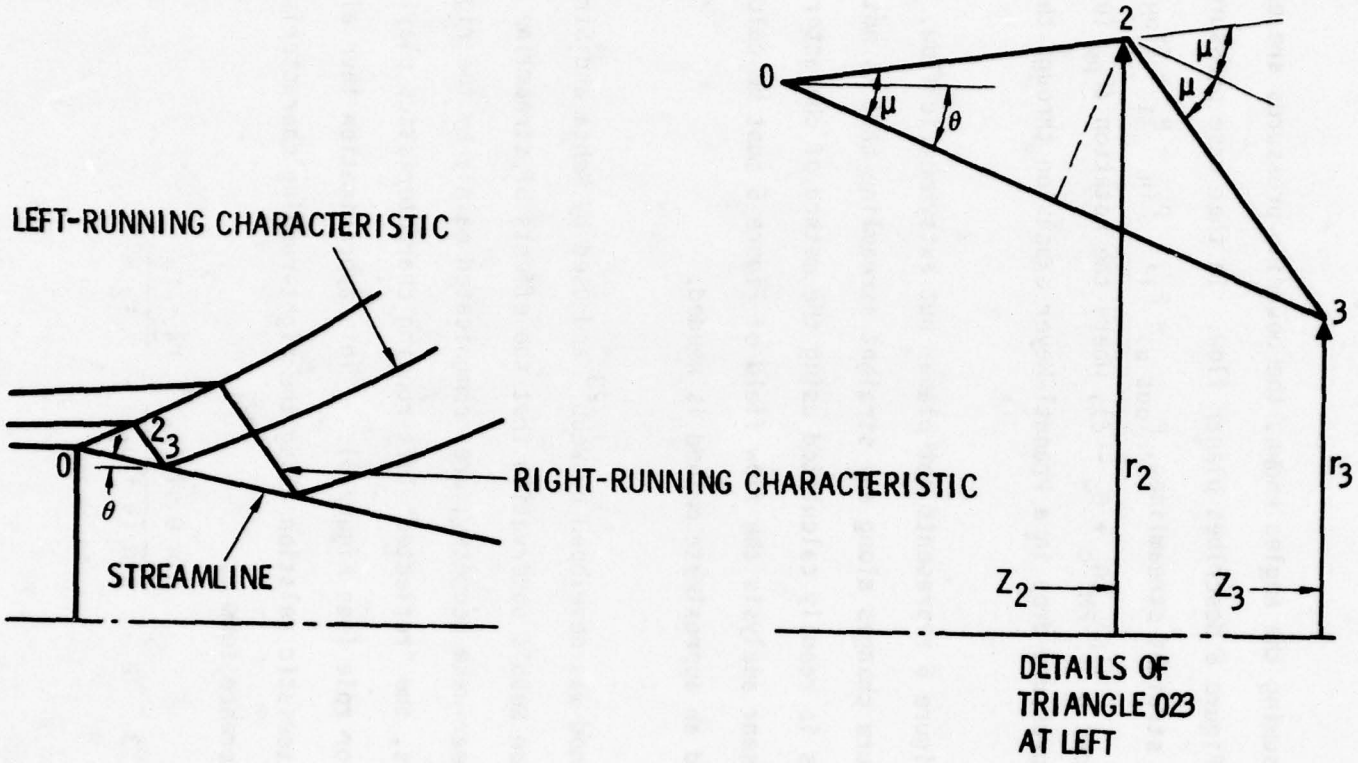

Figure 8. Characteristics Net for Axially Symmetric Near Wake

to give the change in Prandtl-Meyer angle ν as a function of the changes in flow direction θ and radius r, and the Mach angle μ. The numbering and location of points is shown in Figure 8.

Note that (7), applied to the cavity, allows the use of a constant pressure boundary but then results in non-constant direction (the same result Chapman[15] obtained). However, on the basis of observed geometry[15], we take the other option, assuming direction constant (i.e., $\theta_3 - \theta_2 = 0$) and finding $\nu(r)$ and thus $P(r)$.

The term $(r_3 - r_2)/r_2$ in (7) is obtained as follows: from Figure 8, it is clear the following expressions hold:

$$L_{03} = z_3/\cos\theta$$

$$z_3 = (r_0 - r_3)\ \mathrm{ctn}\ \theta$$

$$L_{23} = 1/2\ L_{03}/\cos\mu$$

$$r_2 = r_3 + L_{23}\cos\left(\frac{\pi}{2} - \theta - \mu\right)$$

From these we obtain

$$\frac{r_3 - r_2}{r_2} = \frac{R - 1}{1 + R\left(\frac{2}{A} - 1\right)} \tag{8}$$

where

$$A = \frac{\sin(\theta + \mu)}{\sin\theta\cos\mu} \tag{9}$$

and R = radius, nondimensionalized in such a way that the final value is 1; thus for the inner flow $R = r_3/RW$; for the outer flow upstream of R_{turn}, $R = r_3/R_{turn}$; for the downstream outer flow, $R = r_3/R_3$.

Thus (7), with (8) and (9), gives $\nu(r)$, and the Prandtl-Meyer relation gives P(r). Then average pressures for use in the momentum equation are obtained as follows:

$$PIN = \frac{1}{\pi \left(R_W^2 - R_B^2\right)} \int_{r = \frac{R_B}{R_W}}^{1} 2\pi \; r \; dr \; P(r) \qquad (10)$$

$$POUTU = \frac{1}{\pi \left[R_{turn}^2 - \left(R_B + R_1\right)^2 \right]} \int_{r = \frac{R_B + R_1}{R_{turn}}}^{1} 2\pi \; r \; dr \; P(r) \qquad (11)$$

$$POUTD = \frac{1}{\pi \left(R_3^2 - R_{turn}^2\right)} \int_{r = \frac{R_{turn}}{R_3}}^{1} 2\pi \; r \; dr \; P(r) \qquad (12)$$

Entrainment: The injectant annulus entrains air from the external flow via mixing in the outer shear layer. This mixing is accounted for by inclining the outer boundary of the annulus at an angle σ to the local streamlines; σ is the mixing half-angle defined by the maximum slope of the concentration profile.

(Its relation to the similarity length scale, also often denoted σ, is discussed by Brown and Roshko.[25]) The area through which the entrained flow passes is thus defined, but before its mass flow rate can be obtained, its density and velocity must be known.

These are found from the average pressures, by assuming the flow isentropic. The following relations are used:

$$V_{out\ u} = V_1 \left(\frac{P_{out\ u}}{P_1} \right)^{\frac{\gamma-1}{2\gamma}} \left[\frac{\left(1 + \frac{\gamma-1}{2} M_1^2\right)\left(\frac{P_1}{P_{out\ u}}\right)^{\frac{\gamma-1}{\gamma}} - 1}{\frac{\gamma-1}{2} M_1^2} \right]^{1/2} \tag{13}$$

$$V_{out\ d} = V_2 \left(\frac{P_{out\ d}}{P_2} \right)^{\frac{\gamma-1}{2\gamma}} \left[\frac{\left(1 + \frac{\gamma-1}{2} M_2^2\right)\left(\frac{P_2}{P_{out\ d}}\right)^{\frac{\gamma-1}{\gamma}} - 1}{\frac{\gamma-1}{2} M_2^2} \right]^{1/2} \tag{14}$$

$$(\rho v)_{out\ u} = \rho_1 v_1 \left(\frac{P_{out\ u}}{P_1} \right)^{\frac{\gamma+1}{2\gamma}} \left[\frac{\left(1 + \frac{\gamma-1}{2} M_1^2\right)\left(\frac{P_1}{P_{out\ u}}\right)^{\frac{\gamma-1}{\gamma}} - 1}{\frac{\gamma-1}{2} M_1^2} \right]^{1/2} \tag{15}$$

$$(\rho v)_{out\ d} = \rho_2 v_2 \left(\frac{P_{out\ d}}{P_2} \right)^{\frac{\gamma+1}{2\gamma}} \left[\frac{\left(1 + \frac{\gamma-1}{2} M_2^2\right)\left(\frac{P_2}{P_{out\ d}}\right)^{\frac{\gamma-1}{\gamma}} - 1}{\frac{\gamma-1}{2} M_2^2} \right]^{1/2} \tag{16}$$

In the above, P_1 and M_1 are values outside the annulus at the base plane, while P_2 (and therefore M_2) are calculated from P (R_{turn}), obtained the same way as P(r) in (10) - (12), and then expanded around the corner at R_{turn}.

Mixing Half-Angle σ: Ideally, σ would be determined by analysis of the external shear layer. In 1972, when the Langley Conference[26] on free turbulent shear flows was held, it was known from experiment that for a turbulent shear layer, above a stagnant region, mixing is decreased from the subsonic case when the flow is supersonic. In fact, a reasonably good fit to the data is[14]

$$\sigma = \frac{5}{1 + \frac{\gamma-1}{2} M^2} \tag{17}$$

The ability to calculate this sort of behavior, however, is another matter. Only a few analyses show anything like this Mach number dependence, and though more work has been done on the subject since then,[27] a reliable prediction of σ does not yet exist even for this relatively simple case. The present application is further complicated by including supersonic flows of different gases on either side of the shear layer, vortical structures from the individual jets, and streamwise and transverse pressure gradients. Here we evade these difficulties by leaving σ to be determined.

SECTION THREE

NUMERICAL ASPECTS

Method of Solution

The unknowns in (1) and (2) have now been obtained, leaving one equation for R3, the annulus outer radius at the cone-cylinder transition, but requiring the angles shown in Figure 6. The method of solution is as follows:

(1) A value of δ, the annulus divergence angle, is assumed.

(2) A value of Θ_w is assumed.

(3) From these and the base plane values, PIN and POUTD are calculated.

(4) Adjust Θ_w, at constant δ, until ε_ρ = (PIN-POUTD)/POUTD is sufficiently small.

(5) Set P_{i+1} = (PIN + POUTD)/2 and calculate R3 from equations (1) and (2).

(6) Calculate R3S from the geometry shown in Figure 6.

(7) Adjust δ until ε_{R3} = (R3 - R3S)/R3 is sufficiently small.

A flow chart of the resulting computer program is shown in Figure 9.

Solution Behavior

Multiple Solutions

The formulation required for even the highly approximate version of reality described in the previous paragraphs is, as can be seen above, conceptually simple but mechanically fairly complex. Difficulties have been encountered in obtaining solutions under some sets of conditions. In this section we discuss some of these problems.

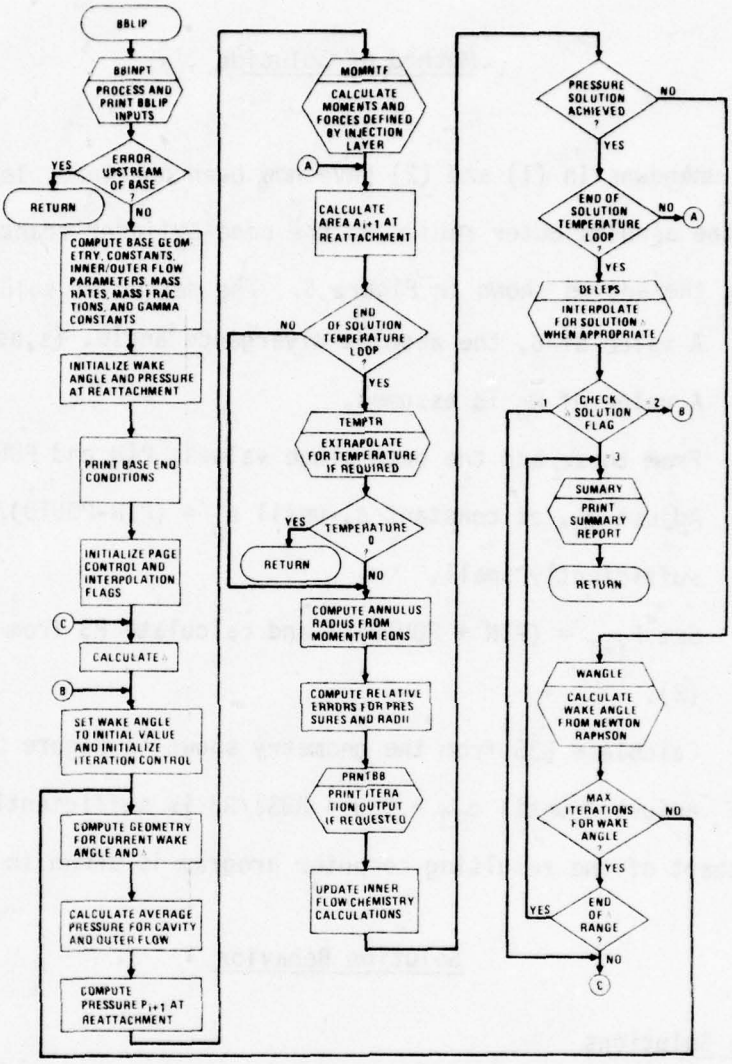

Figure 9. Flow Chart of Computer Program

Whatever the cause, the problem most often seen shows up as multiple solutions, or as a failure to reach a solution. Referring to the simplified solution outline presented above, what often happens is the following. Steps (1) - (4) can usually be completed without difficulty, as can steps (5) and (6), which are purely mechanical. But either no δ, or more than one, can sometimes be found to satisfy step (7).

Now it seems clear that neither no solution, nor probably multiple solutions, can correspond to physical reality. However, this difficulty is believed to be related to the physics, possibly as follows. Consider PIN and POUTD, which are forced to match by adjusting θ_w and δ. (It is found that θ_w and δ are linearly related, so it suffices in this discussion to talk in terms of one of them, say θ_w.) In this way the geometry is obtained, which then yields an exit radius R3S and allows calculation from the conservation equations of another, R3, which must match it.

But PIN and POUTD are decreasing functions of θ_w. Both result from expanding different flows (respectively the injectant and external flows), and often from nearly the same value. (These initial values will be the same if the annulus streamlines upstream of the turning ray or expansion are parallel to the centerline, because by the upstream individual-jet calculation, inner and outer-flow pressures are forced to be equal at the base plane.) If the expansion begins at the same value, and if the functions $P(\theta_w)$ are similar, no solution can exist (Fig. 10). If the functions are dissimilar, one, two, or no solutions can exist, as that Figure shows.

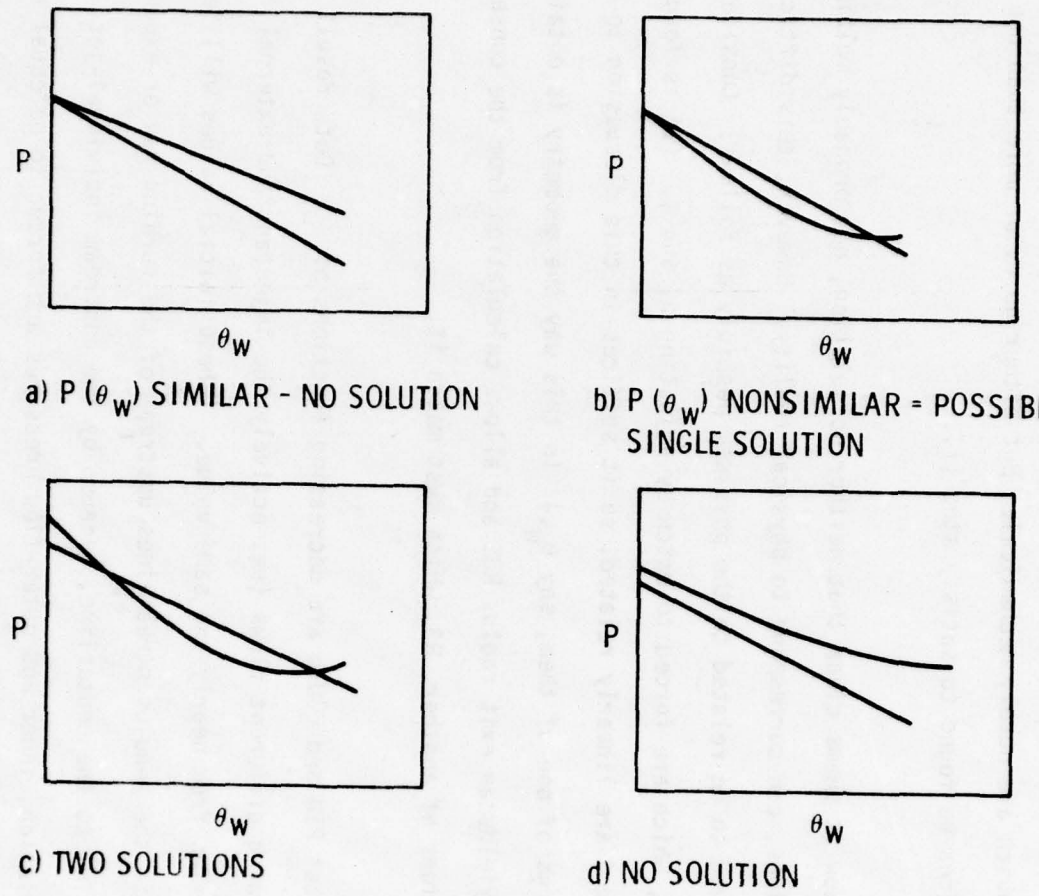

Figure 10. Examples of Possible Solution Behavior

Different behavior would be found if one of the two functions were an increasing function of θ_w. As it is, we may expect difficulties with stability as well as number of solutions; Figure 10(c) shows an example where the solution(s) would change substantially with a very small change in initial conditions or functional dependence.

An example of multiplicity or absence of solutions is shown in Figure 11, which shows ε_{R3} as a function of δ. As shown, single solutions seem to exist for M = 2 and M = 5, and no solutions for M = 2.5, 3 and 3.5. However, Figure 11 (as noted there) is for σ = 0.6 deg., and it has been found that varying σ has the effect of translating the whole pattern up or down (increasing σ moves the pattern down) without changing its character. In particular, an increase in σ might bring the pattern far enough down that line b in Figure 11 would coincide with $\varepsilon_{R3} = 0$. If that were the case, Figure 11 would show a single solution for M = 2, multiple solutions for M = 3 and 3.5, and probable multiple solutions for M = 2.5 and 5.

These solutions can be denoted plus and minus solutions, based on the sign of $d\varepsilon_{R3}/d\delta$. Thus the single solution for M = 2 is a plus solution, and that for M = 5 is a minus solution. In fact the above discussion implies that we can often, perhaps always, adjust σ to obtain two solution branches over much of the Mach number range. The "correct" branch might then be chosen by some as yet undetermined means.

But when this is done, two observations are made. First, only the plus solution can be reached at Mach 2, and only the minus at Mach 5. A jump in

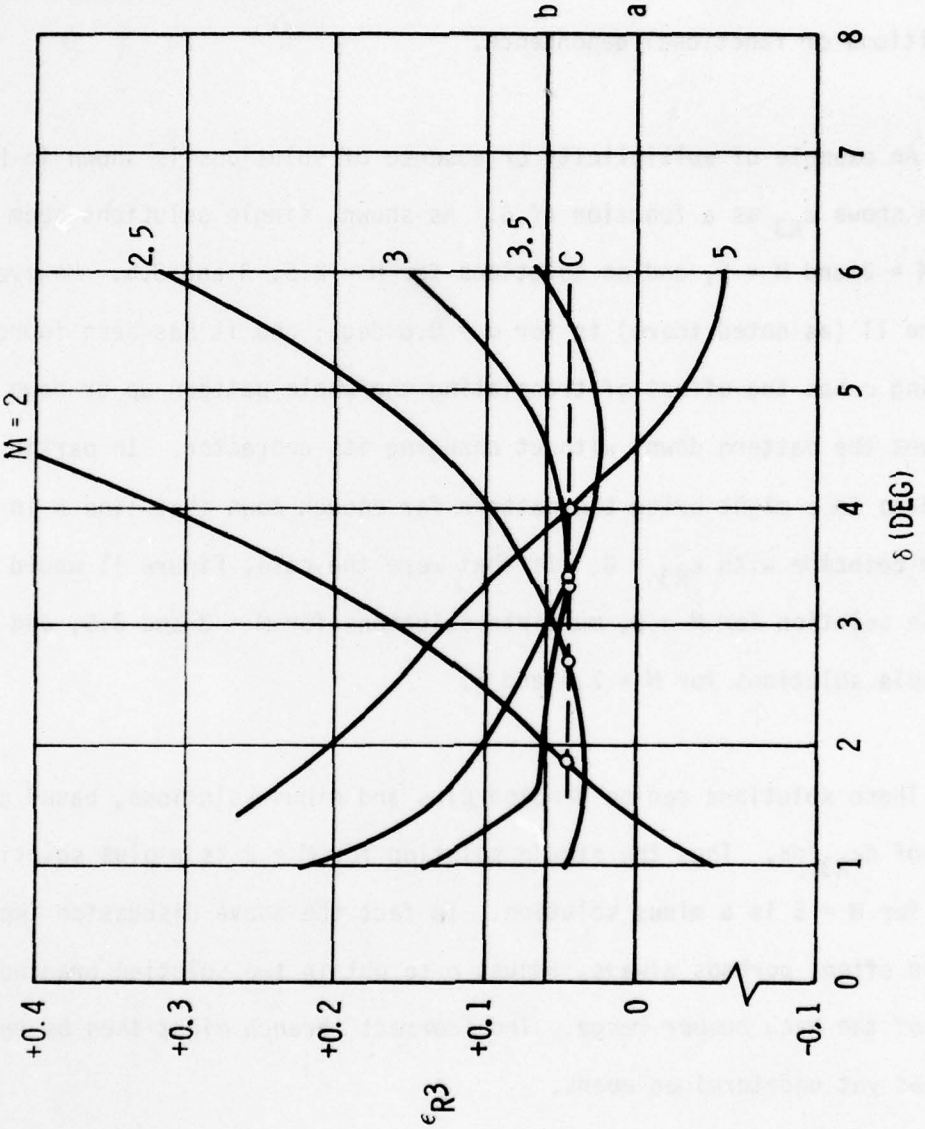

Figure 11. Typical Solution Behavior (σ = 0.6 Deg)

base pressure results on transition from one solution to the other and as both solutions exist over a wide range, transition is not uniquely located. Second, neither solution really behaved right, both in terms of P(M) and of θ_w (M). Observation of shadowgraphs for a wide range of conditions showed $10 < \theta_w < 15$ degrees. This is without injection, and yet it is believed that the same range should be seen with injection, at least in the absence of very large heat release. Neither solution branch stays in the correct θ_w range over the whole Mach number range.

Another option exists, typified by the dashed line labeled "C" in Figure 11. A single solution can be made to exist over the whole range of Mach numbers, by adjusting the pattern shown in Figure 11 so that the curve with the highest minimum (in Figure 11 it is the one corresponding to Mach 3) to be tangent to the $\varepsilon_{R3} = 0$ line. We now have one solution, and only one, at the corresponding Mach number; and this means there is one continuous solution over the whole Mach number range. The tangency condition has in fact produced a transition between plus and minus solutions at the point of tangency.

As will be seen when results are disclosed, this approach is not without attractions. It produces reasonable answers for both base pressure and wake angle over the whole Mach number range (although it will be seen that not all the trends predicted are so reasonable). Before looking at results, however, two questions need to be discussed.

First, though this approach appears expedient, it is justifiable? Is the answer thus obtained the correct answer? The answer to this question is not known. Mathematically speaking, no proof of uniqueness is advanced here. Considering the approximations involved and the nonlinearity of the resulting formulation, such a proof may be impossible to obtain and might, if obtained, be meaningless.

Physically, at each set of vehicle, flight and injection conditions, a solution must exist. More than one may exist, or transitions may exist. Although there is some evidence suggesting both can occur under at least some conditions,[28] it seems probable that base pressure or any geometrical variable is a continuous function of any of the independent variables. Insofar as the approach under discussion produces continuous results, it appears justified in this limited sense.

Second, how can the pattern be adjusted? It is known that this can be done by changing the mixing half-angle σ. However, σ cannot be changed freely. There is evidence that σ depends on the Mach numbers and densities of the flows bounding the shear layer[25] (see also the discussion in Section II above), and that σ decreases downstream of individual lateral jets,[11, 12, 13] presumably as the turning vortices die away. Other changes in σ cannot be justified, and if they are required in order to produce continuous results, the entire method comes under suspicion.

It is believed that there is another way of adjusting the pattern: by changing ϕ_b, the external, upstream divergence angle (Figure 6). At present

this change is only possible in principle, as ϕ_b is included in the external flow formulation in such a way as to preclude negative values, and is not included in the annulus flow formulation at all. However, it is believed that this is an area where continued work might be fruitful.

Radial Momentum

Conservation of axial momentum is required, as described above (Equation (1)), but radial momentum is left to fend for itself. The change in pressures as streamlines change direction should account for radial momentum conservation. This is true, for example, in a Prandtl-Meyer expansion in planar flow, or in an axisymmetric flow calculated by the method of characteristics. In the present case an approximation to the method of characteristics is used, and the amount of error involved in the approximation is not known. The degree to which radial momentum is conserved gives an estimate of the errors involved.

This is done as follows. The component terms of the radial momentum equation are calculated:

$$
\begin{aligned}
\text{PAROU} &= \text{POUTU} * A(r, z, \theta) \\
&\quad \text{where } A(r, z, \theta) = 2\pi rz + \pi z^2 \tan\theta \\
&\quad \text{and } r = \text{RBRI} \\
&\quad\quad z = \text{LTURN} \\
&\quad\quad \theta = \phi_c + \phi_b + \sigma \\
\text{MVROU} &= -\text{DMDTUP} * \text{VOUTUP} * \sin(\theta_c + \phi_b) \\
\text{PAROD} &= \text{POUTD} * A(\text{R3S}, \text{HL-LTURN}, \theta_w - \delta - \sigma) \qquad (18) \\
\text{MVROD} &= \text{DMDTDN} * \text{VOUTDN} * \sin(\theta_w - \delta) \\
\text{MVREX} &= -\dot{m}_{i+1}, v_{i+1}, \sin\left(\theta_w - \frac{\delta}{2}\right)
\end{aligned}
$$

$$\text{PARIN} = -\text{PIN} * A(RW, HL, \theta_w)$$

$$\text{MVRINL} = -\dot{m}_i v_i \sin(\theta_c + \phi_b) \qquad \text{(18 cont.)}$$

Then, to estimate the degree by which we fail to conserve angular momentum, we calculate

$$\text{RMOMCK} = \frac{\text{algebraic sum of above terms}}{\text{sum of absolute values of above terms}} \qquad (19)$$

Values of RMDMCK at solutions range from 0.17 to 0.05, with no trend evident from which systematic errors can be deduced. The values seem reasonably small, and not inconsistent in absolute value with the approximations made in the analysis and described above. The fact that only positive values of RMOMCK are seen seems to indicate that the negative terms in the numerator of (19) are too small. Since PARIN dominates the negative terms, conservation of radial momentum would be well approximated by multiplying PIN -- and therefore PB -- by a factor (1 + RMOMCK). This cannot be done so simply, as it would upset the other conservation equations that have already been satisfied; nevertheless it is probably an indication that the base pressure we calculate is slightly too low.

SECTION FOUR

COMPARISON WITH DATA

Only one set of unclassified data exist for gaseous injectant and axisymmetric geometry.[4] The data labeled ARC on Figure 12 include only those low-altitude, low-M_∞ points that are claimed by the authors of Reference 4 to be free of tunnel interference effects. This conclusion may be questioned because it appears that a reflected jet shock would cross the wake axis upstream of reattachment, and because their measured lip pressures appear too high. Some question also exists because P_B/P_∞ appears independent of $\dot{m}_j$ over a substantial range. Nevertheless, it is the only unclassified result available.

Considerable data exist for base pressure without injection. These are shown in Figure 12 as the "$\dot{m}_j = 0$ data range." These data show some evidence of an inflection point similar to that shown between Mach 3 and 4 by the present calculations, and the general shape is not dissimilar to that resulting from the present calculations.

In Figure 12 these data are compared with results of the present model. The comparison is not exact, in the sense that somewhat different conditions were used in the calculation than were present in the experiment. Conditions used in the calculations are shown in Table 1, with $P_\infty = 200$ lb/ft^2. There are several reasons for this. The ARC data involved a propellant for which the details of composition were not readily available, and the questions underlying the validity of the data made it appear that only an approximate

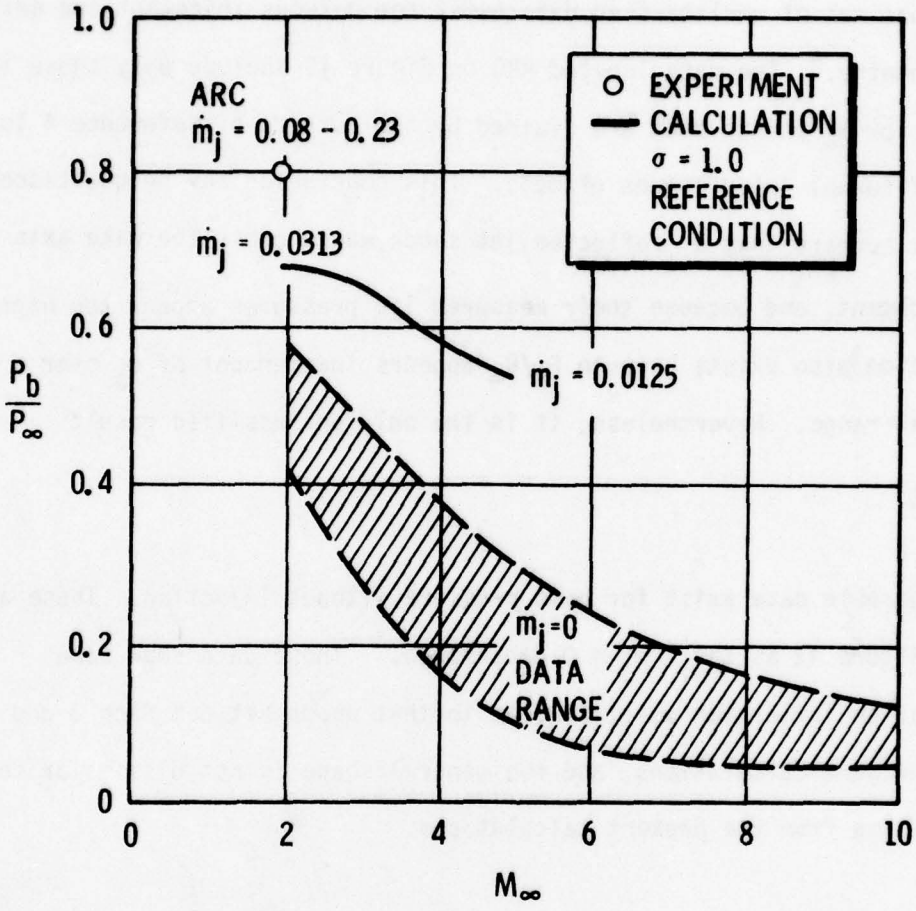

Figure 12. Comparison of RW > 0 Calculations with Experimental Data

Table 1: PROGRAM INPUTS: REFERENCE INPUTS

VEHICLE PARAMETERS:				
FIRST HALF CONE ANGLE	THETA1	=	6.00	DEGREES
SECOND HALF CONE ANGLE	THETA2	=	.01	DEGREES
LENGTH OF VEHICLE	XBODY	=	3.75	FEET
LENGTH OF CONE	YCONE	=	2.75	FEET
THRUSTER ANGLE	THETAJ	=	.00	DEGREES
FLIGHT PARAMETERS:				
TEMPERATURE	TINF	=	390.00	DEGREES RANKINE
ANGLE OF ATTACK	ALPA	=	0.00	DEGREES
BANK ANGLE	PHI	=	0.00	DEGREES
VEHICLE CENTER OF GRAVITY	ICG	=	1.83	FEET (MEASURED FROM NOSE)
RATIO OF SPECIFIC HEATS	GAMA	=	1.40	(DIMENSIONLESS)
INJECTOR PARAMETERS:				
CHAMBER PRESSURE	POJET	=	50.00	POUNDS PER SQUARE INCH ABSOLUTE
THROAT AREA	AOJET	=	.03	SQUARE INCHES
EXPANSION RATIO	ERATIO	=	2.00	(DIMENSIONLESS)
INCLINATION OF JET	ALFAJ	=	-51.00	DEGREES
INJECTOR SITE DISTANCE	ZJET	=	1.60	INCHES (MEASURED FROM VEHICLE BASE)
HALF ANGLE OF NOZZLE EXIT CONE	BETA	=	15.00	DEGREES
PROPELLANT:				
FUEL	NUMBER		19	ARCADENE 168(ARC TESTS)
OXIDIZER	NUMBER		19	ARCADENE 168(ARC TESTS)
OXIDIZER-FUEL RATIO	OOVERF	=	1.00	(DIMENSIONLESS)
PROGRAM FLOW PARAMETERS:				
FROZEN/EQUILIBRIUM CHEMISTRY	ETAR	=	0.00	(DIMENSIONLESS)
NOSE RADIUS MULTIPLIER	PCTR	=	.8000	(DIMENSIONLESS)

comparison would be justified. Because of the essential nature of the injectant annulus in the calculation, no runs without injection can be made, and thus only a qualitative comparison with the no-injection data can be made. Considering these limitations, the agreement shown in Figure 12 is believed to be reasonably good.

SECTION FIVE

PARAMETRIC SURVEY

Parameters Studied

A large number of inputs are required for the calculations described above. Most of these are shown in Table 1, which also shows the values of these inputs that are taken as reference conditions for the parametric survey. Table 2 shows the parameters to be varied, and the ranges desired.

From Table 1 and Figure 13, the vehicle is seen to be a biconic, 3.75 ft. long overall. The nose is a 6 deg. half-angle cone, followed by an almost-cylindrical section (0.01 deg. half-angle), 1 ft. long. (The program cannot use a body half-angle of zero.)

The atmosphere is assumed, for purposes of this study, to have a constant temperature of 390 R.

Effect of Parameters

Mach Number and Altitude

The effect of flight Mach number is shown in Figure 14. For a range of altitudes, the continuous variation of P_B/P_∞ with M_∞ is a result of enforcing transition between plus and minus solutions as described above. The mixing half-angle required for this transition was $\sigma = 1.0$ deg. This is an eminently reasonable value -- an incompressible shear layer with one side bounded by stagnant fluid has $\sigma \sim 6$ deg., and both $M > 0$ and $U_2 > 0$ (sub 2 denoting the low-speed side) are known to decrease σ.

Table 2. PARAMETERS TO BE VARIED (INCLUDING DESIRED RANGES)

1. Local Mach number (2 to 5; lower limit of 1.5 if possible)

2. Altitude (sea level to 100K ft)

3. Propellant mass flowrate

4. Missile diameter (base diameter from 2 to 16 in)

5. Propellant type (solids with and without Al; liquid bipropellant; monopropellant liquid; GH_2)

6. Injector location on missile body

7. Injection momentum

8. Number of injectors (from 2 to a number sufficient to approximate an annulus)

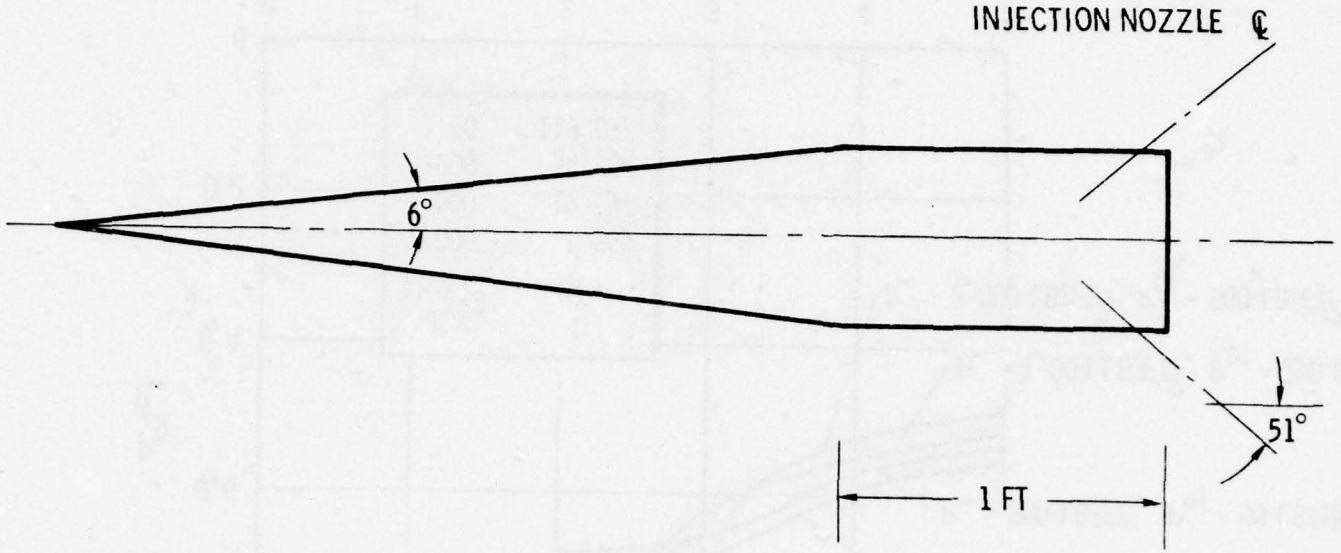

Figure 13. Basic Vehicle for Parametric Survey (Approximately to Scale)

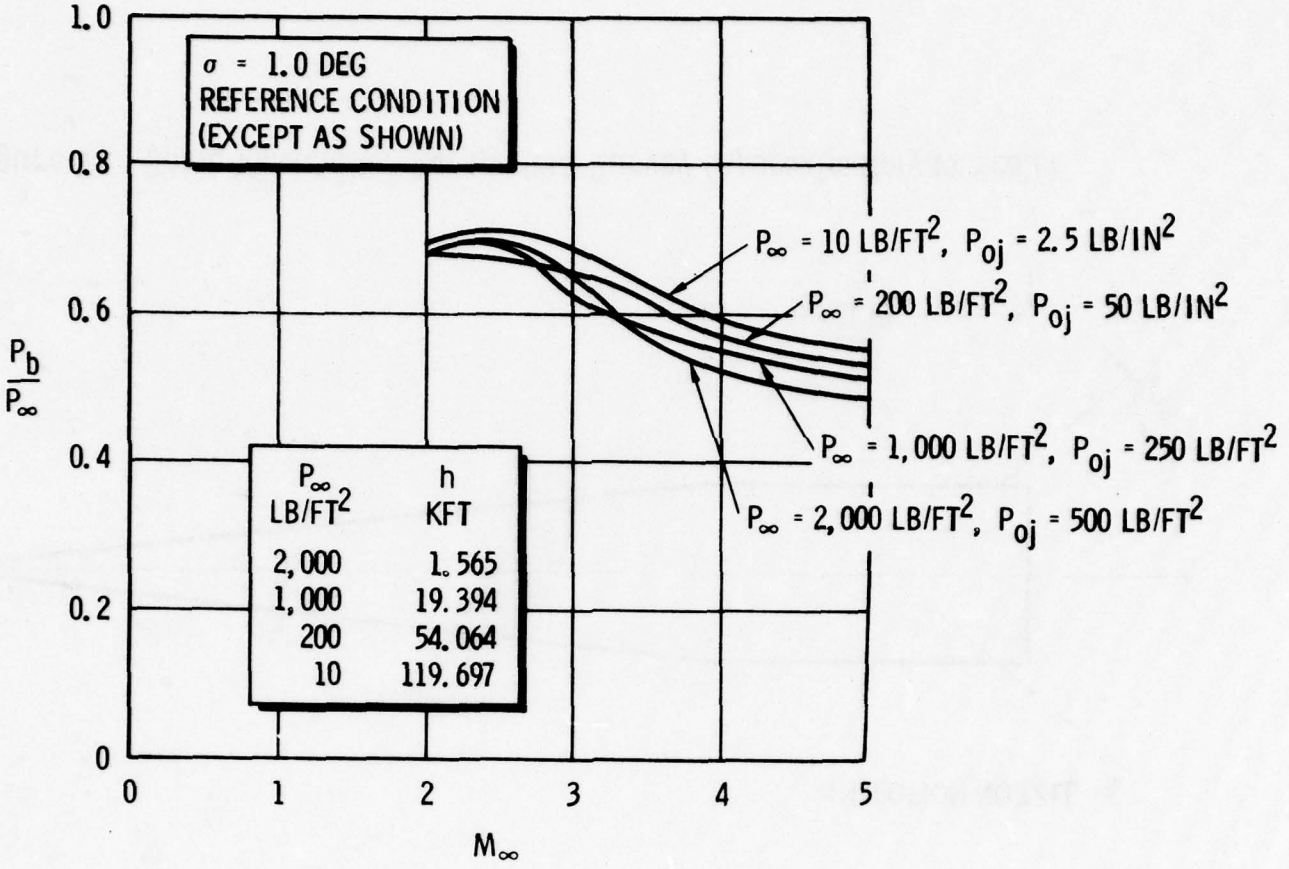

Figure 14. Effect of Flight Mach Number

Table 2 shows an altitude range of sea level to 100,000 ft is desired. In terms more consonant with the inputs of the present program, this corresponds to ambient pressures in the approximate range $2000 < P_\infty < 20$ lb/ft^2. Calculations cannot be made for a single vehicle with fixed injection conditions flying over this range. This is because at relatively high values of P_∞ ("relative" refers to the jet total pressure P_{oj}) the injectant flow will separate within the injectant nozzle, while at low P_∞ the individual jets produce such large disturbances that the jets are not turned downstream, even approximately, by the time the base plane is reached.

Thus the desired altitude range can only be covered by varying P_{oj} with P_∞, so as to stay within the range for which calculations can be made. Because of the importance of altitude as a parameter, these calculations are made over the entire Mach number range. Results are shown in Figure 14.

Several aspects of these results are of interest. First, it appears that the case chosen to show the effect of Mach number in Figure 12, the choice being made because $P_\infty = 200$ lb/ft^2 corresponds to an altitude intermediate in the desired range, was somewhat unique in that performance at all other pressures is increasing with Mach number at $M_\infty = 2$. It is not clear whether this trend is a real one, or an artifact of the approximations used.

Second, performance is highest at the highest altitude. This does not include combustion, and since P_{oj} is scaled with P_∞ we might expect identical performance to be obtained here (and in fact over the whole range).

The difference is believed to arise from the use of fully equilibrium chemistry to obtain jet conditions in the individual-jet calculation.

Injectant Mass Flow Rate

This important parameter can be varied in more than one way. Two of the simplest were chosen for the present survey: variation of jet throat area A_{ojet} and of jet total pressure P_{ojet}. Results of varying these inputs are shown in Figure 15, for $M_\infty = 2$ and $\sigma = 1.0$ deg, and for the reference conditions of Table 1.

Several interesting things can be seen from this Figure. Variation of $\dot{m}_j$ by the two methods has opposite effects. This is consistent with existing data, which indicate that low-velocity injection is most effective for a unit of mass flow,[14, 29] and which may be interpreted as meaning that the best performance is reached by disturbing the external stream least.

The behavior of P_B/P_∞ as $\dot{m}_j \to 0$ is of interest. The data range for $\dot{m}_j = 0$ is shown on the ordinate in Figure 15. As $A_{ojet} \to 0$ the computed P_B/P_∞ is clearly approaching a value that will at least approximately agree with experiment; just as clearly, when $P_{ojet} \to 0$, the correct limiting value will be reached only by what seems to be an improbable change in shape of the curve. This behavior is so far unexplained and needs an explanation.

Finally, Figure 15 also shows a large scatter. All points shown are actual calculations. This sort of scatter did not occur in runs over the Mach number or altitude ranges previously discussed, and to find it here is an unpleasant surprise. Its cause is not clear. Numerical solutions can be expected to

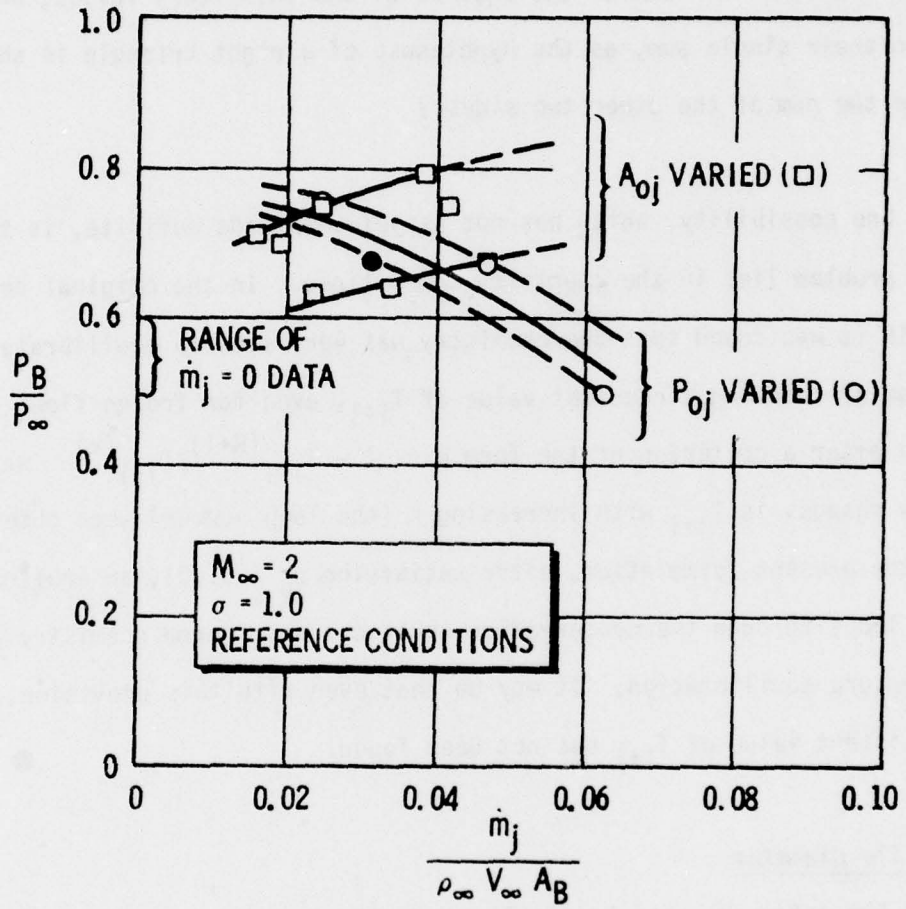

Figure 15. Effect of Injectant Mass Flow Rate

show scatter of the order of the convergence criteria; but here 0.1% is used, and we observe scatter of order 10%. Of course a number of such criteria must be satisfied, but even neglecting their almost certain independence and summing their effects can account for less than an order of magnitude increase in scatter, leaving another order of magnitude to be accounted for. (The scatter caused by a number of truly independent sources is found as the square root of the sum of the squares of the individual values, which is less than their simple sum, as the hypotenuse of a right triangle is shorter than the sum of the other two sides.)

One possibility, which has not as yet been made definite, is that part of the problem lies in the chemistry subroutines. In the original development of BBLIP it was found that the chemistry was very slow to equilibrate, in the sense of reaching a constant value of T_{i+1}, even for frozen flow; and that even after a criterion of the form $\varepsilon = 1 - T_{i+1}^{(R+1)}/T_{i+1}^{(k)}$ was satisfied, slow changes in T_{i+1} with increasing k (the loop number) were observed. Even in the present formulation, after satisfying $\varepsilon_p < 0.001$, an arbitrarily chosen 100 loops through the conservation equations and thermo chemistry are made to ensure equilibration. It may be that even with this provision, a fully consistent value of T_{i+1} has not been found.

Missile Diameter

The reference vehicle (Table 1 and Figure 13) is a biconic that approximates a cone-cylinder; the nose is a 6 deg. half-angle cone, 2.75 ft. (33 in.) long, and the "cylindrical" section is actually a 0.01 deg. half-angle cone, one foot long. (The "cylindrical" section thus diverges by

0.00209 in. in radius.) The reference base diameter is 6.936 in. To vary the base diameter over the desired range we vary the cone length over the range (in feet) 0.833 < XCONE < 6.67.

If all lengths in the problem are scaled to keep geometrical similarity, the same base pressure would result. This is also approximately true if the "cylindrical" section length is held fixed as other lengths change, since although local conditions are affected by the proximity of the conical section, this effect is not large. We therefore take the more difficult route of holding all other variables constant while XCONE is varied. When this is done, Figure 16 results. It shows base pressure increasing with decreasing base diameter. This can be viewed as equivalent to an increase in the nondimensional injection flowrate $\dot{m}_j/\rho_\infty v_\infty A_B$; as shown in Figure 16, a base diameter of 2 in. yields, with the reference conditions of Table 1, a nondimensional injection rate of 0.207. This method of changing flowrate may be considered equivalent to changing A_{ojet}, since the jet velocity is not changed in either case (see the discussion above). If so, we can combine the data shown in Figures 15 and 16 to yield the result shown in Figure 17.

No line is drawn through the different regions in Figure 17, as they were obtained by different methods and it is not certain that comparison is valid. Nevertheless, if one were known, its shape would be quite reasonable. Its slope would be proportional to specific impulse, and would clearly be greater at low than at high injection rate. This is consistent with all experience in this and similar areas. It would apparently require very substantial injection to raise the base pressure above ambient, and this too is consistent

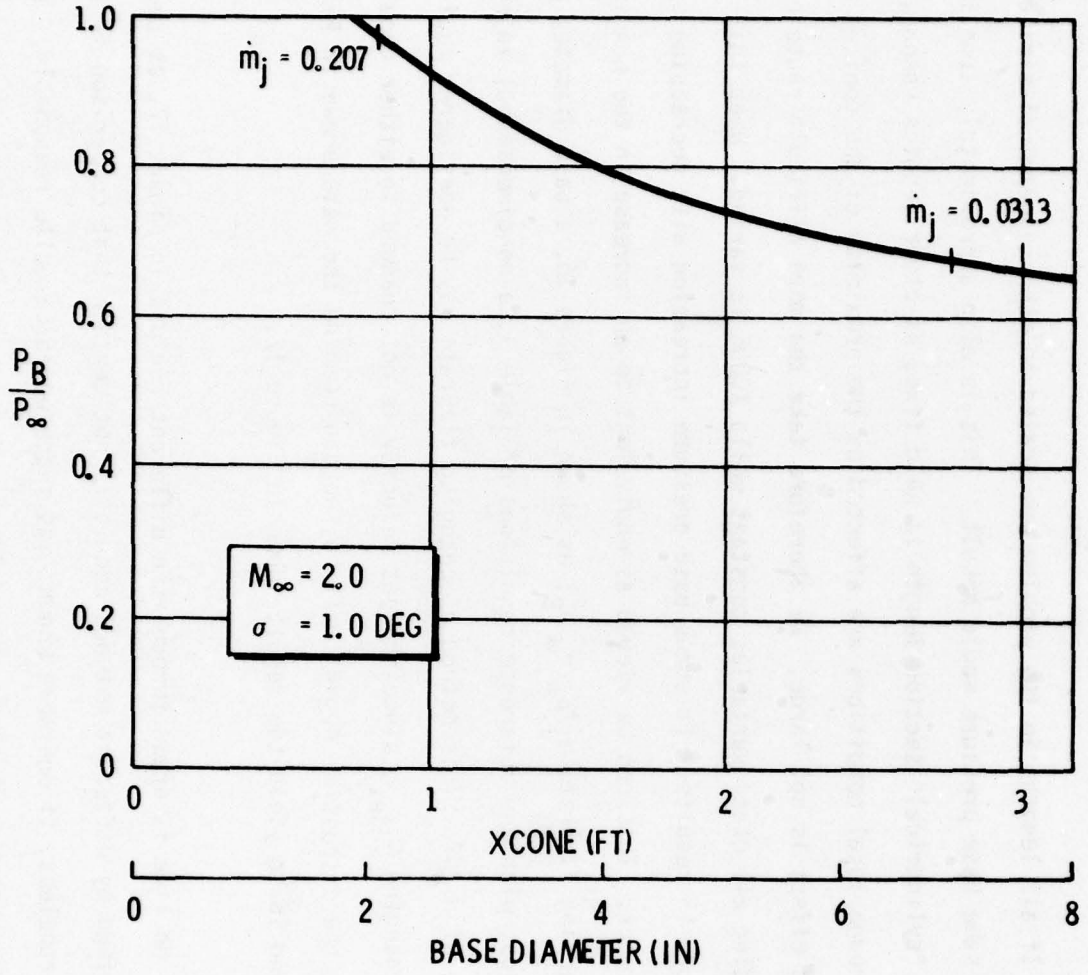

Figure 16. Effect of Vehicle Base Diameter (Cone Length Varied, Other Parameters Constant)

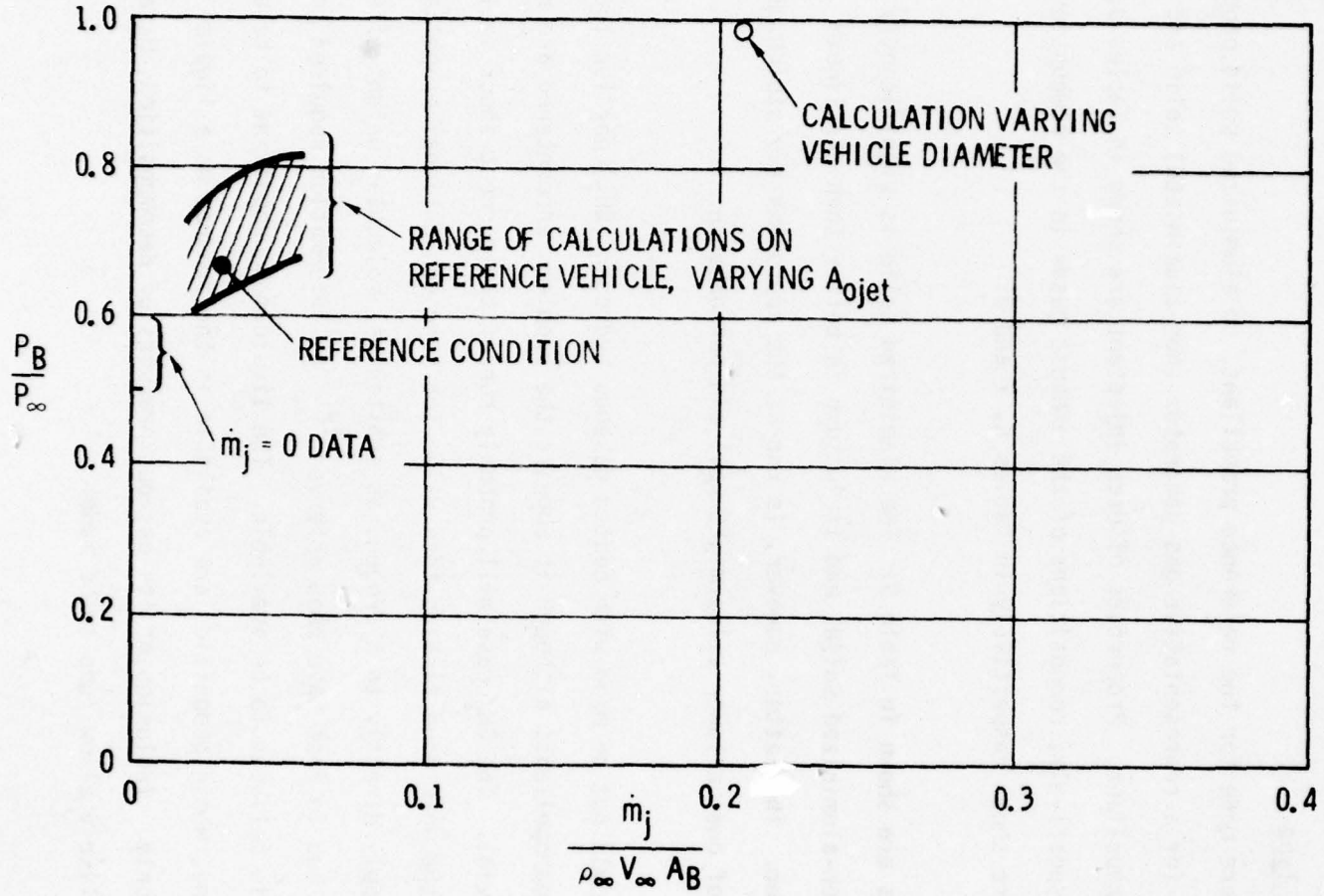

Figure 17. Effects of Varying Nondimensional Injection Rate by Different Means

with expectations.

Propellant Type

Runs were made for the reference propellant, an aluminized solid propellant, as well as for a representative gas generator (non-aluminized) solid and a liquid bipropellant. Properties of each injectant are shown in Tables 3, 4 and 5 respectively; compositions of the exhaust gases in the combustion chambers are shown respectively in Tables 6, 7 and 8.

Results are shown in Table 9. The aluminized solid is significantly better than the non-aluminized solid, and it in turn is better than the liquid bipropellant. The latter, however, is run at the approximately stoichiometric O/F ratio of one; a lower value might well aid performance.

Runs could not be made with heated gaseous hydrogen (GH_2) nor for the liquid monopropellant, although it appears the problems encountered are relatively trivial. The GH_2 case will probably run if the correct shock scale can be found; the work done finding this value for more conventional propellants does not apply directly to hydrogen, as substantial molecular weight effects are likely and in fact have been observed.[19] The information required to repeat this work is believed to be available. The liquid monopropellant to be used is hydrazine, whose properties are available in the program as a liquid injectant only. Inclusion of its gaseous products of decomposition, H_2 and N_2, will very likely allow runs to be made.

Table 3. REFERENCE PROPELLANT

JET CONDITIONS:

MACH NUMBER	MJET	=	1.9781	(DIMENSIONLESS)
EXIT TEMPERATURE	TJET	=	2313.68	DEGREES RANKINE
EXIT VELOCITY	VJET	=	5587.27	FEET/SECOND
EXIT DENSITY	ROJET	=	.0001396	SLUGS/CUBIC FOOT
MOLECULAR WEIGHT	MOLWTJ	=	31.047	(DIMENSIONLESS)
RATIO OF SPECIFIC HEATS	GAMAJ	=	1.1963	(DIMENSIONLESS)
JET THRUST	FR	=	11.48	POUNDS
JET MASS FLOW RATE	MDOTJ	=	.06	POUNDS/SECOND

JET THERMOCHEMISTRY:

TOTAL ENTHALPY		
PROPELLANT	-362.620	CAL/GRAM
PRODUCTS	-1434.603	CAL/GRAM
HEAT RELEASE	1091.983	CAL/GRAM
EXIT ENTHALPY	-709.037	CAL/GRAM
SPECIFIC HEAT	.39012	CAL/GRAM/DEG K

Table 4. NON-ALUMINIZED SOLID PROPELLANT

JET CONDITIONS:

MACH NUMBER	MJET	=	1.9991	(DIMENSIONLESS)
EXIT TEMPERATURE	TJET	=	971.25	DEGREES RANKINE
EXIT VELOCITY	VJET	=	4916.93	FEET/SECOND
EXIT DENSITY	ROJET	=	.0001839	SLUGS/CUBIC FOOT
MOLECULAR WEIGHT	MOLWTJ	=	19.057	(DIMENSIONLESS)
RATIO OF SPECIFIC HEATS	GAMAJ	=	1.3264	(DIMENSIONLESS)
JET THRUST	FR	=	1.95	POUNDS
JET MASS FLOW RATE	MDOTJ	=	.01111	POUNDS/SECOND

JET THERMOCHEMISTRY:

TOTAL ENTHALPY		
PROPELLANT	-424.480	CAL/GRAM
PRODUCTS	-961.359	CAL/GRAM
HEAT RELEASE	536.879	CAL/GRAM
EXIT ENTHALPY	-692.760	CAL/GRAM
SPECIFIC HEAT	.42377	CAL/GRAM/DEG K

Table 5. LIQUID BIPROPELLANT: NITROGEN TETROXIDE/ MONOMETHYL HYDRAZINE (O/F = 1.0)

JET CONDITIONS:

MACH NUMBER	MJET	=	2.0952	(DIMENSIONLESS)
EXIT TEMPERATURE	TJET	=	1464.64	DEGREES RANKINE
EXIT VELOCITY	VJET	=	6677.35	FEET/SECOND
EXIT DENSITY	ROJET	=	.0001004	SLUGS/CUBIC FOOT
MOLECULAR WEIGHT	MOLWTJ	=	16.752	(DIMENSIONLESS)
RATIO OF SPECIFIC HEATS	GAMAJ	=	1.2981	(DIMENSIONLESS)
JET THRUST	FR	=	1.94	POUNDS
JET MASS FLOW RATE	MDOTJ	=	.00823	POUNDS/SECOND

JET THERMOCHEMISTRY

TOTAL ENTHALPY		
PROPELLANT	114.500	CAL/GRAM
PRODUCTS	-931.425	CAL/GRAM
HEAT RELEASE	1045.925	CAL/GRAM
EXIT ENTHALPY	-380.276	CAL/GRAM
SPECIFIC HEAT	.51649	CAL/GRAM/DEG K

Table 6. REFERENCE PROPELLANT: CHEMICAL COMPOSITION OF PRODUCTS

SPECIES	MOLE PERCENT	WEIGHT PERCENT
H2	48.4507	3.1461
CO	24.8259	22.3980
ALCL	13.2544	26.6549
AL2O3*	9.6359	31.6444
N2	7.1218	6.4264
AL	2.6498	2.3027
AL2O	1.8733	4.2211
H	1.0867	.0353
AL2O3$	.549926E+00	.180597E+01
ALCL2	.279025E+00	.879782E+00
HCL	.250906E+00	.294688E+00
ALH	.160925E+00	.145068E+00
CNH	.300251E-01	.261372E-01
H2O	.769029E-02	.446249E-02
CL	.405249E-02	.462807E-02
ALOCL	.302404E-02	.763983E-02
CO2	.684904E-03	.970883E-03
ALO	.406398E-03	.562592E-03
C2H2	.201017E-03	.168584E-03
ALCL3	.166592E-03	.715529E-03
CHO	.113141E-03	.105750E-03
CH4	.600399E-04	.310243E-04
CH3	.485094E-04	.234912E-04
NH3	.418640E-04	.229658E-04
HO	.290862E-04	.159337E-04
AL2O2	.218865E-04	.605966E-04
CN	.938452E-05	.786463E-05
NH	.673214E-05	.325599E-05
NH2	.546039E-05	.281819E-05
ALN	.369861E-05	.488282E-05
CH2O	.324710E-05	.314039E-05
N	.178230E-05	.804142E-06
ALHO	.779190E-06	.110396E-05
NO	.585203E-06	.565613E-06
O	.425825E-06	.219446E-06
ALC	.201274E-06	.262771E-06
CH2	.134244E-06	.606505E-07
C2N2	.109581E-06	.183667E-06
C	.710821E-07	.274989E-07
C2H4	.679077E-07	.613606E-07
CH	.678209E-07	.284392E-07
CL2	.164527E-07	.375790E-07

Table 7. NON-ALUMINIZED SOLID PROPELLANT

CHEMICAL COMPOSITION OF PRODUCTS

SPECIES	MOLE PERCENT	WEIGHT PERCENT
H2	39.6783	4.1974
CO	33.1352	48.7028
HCL	11.3475	21.7126
N2	6.1972	9.1105
CO2	5.0540	11.6715
H2O	3.6153	3.4178
CH4	.970899E+00	.817158E+00
C$	.584828E+00	.368590E+00
NH3	.167865E-02	.150024E-02
CNH	.859082E-04	.121827E-03
CH2O	.757954E-05	.119424E-04
CH3CL	.620245E-05	.164332E-04
C2H4	.3494868-05	.514470E-05
CH3	.159218E-06	.125612E-06
H	.103375E-06	.546782E-08
CL	.282314E-07	.525255E-07
CHO	.248111E-07	.377802E-07
C2H2	.232478E-07	.317633E-07

Table 8. LIQUID BIPROPELLANT: NITROGEN TETROXIDE/ MONOMETHYL HYDRAZINE (O/F = 1.0)

CHEMICAL COMPOSITION OF PRODUCTS

SPECIES	MOLE PERCENT	WEIGHT PERCENT
H2	38.8847	4.6795
N2	27.2821	45.6258
H2O	15.6523	16.8331
CO	15.5993	26.0832
CO2	2.5800	6.7781
H	.116831E-02	.702982E-04
NH3	.290985E-03	.295843E-03
CNH	.131782E-04	.212575E-04
HO	.121523E-04	.123378E-04
CH4	.662916E-05	.634849E-05
CH2O	.191991E-05	.344127E-05
CHO	.162026E-05	.280669E-05
NO	.106044E-06	.189955E-06
NH2	.619373E-07	.592446E-07

Table 9. EFFECT OF PROPELLANT TYPE

$M_\infty = 2.5$

$\sigma = 1.0$

REFERENCE CONDITIONS

Propellant Type	P_B/P_∞
Reference Solid	0.67
Non-Aluminized Solid	0.60
Liquid Bipropellant (NTO/MMH, O/F = 1.0)	0.51

Injector Location

The streamwise location of injection nozzles is a likely field for optimization. The present program cannot treat nozzles nearer the base than 1.33 h, where h is the jet "penetration;" nor can it treat nozzles so far upstream that the individual-jet shock is too close to the Mach angle. The former is a fundamental limitation (although the factor 1.33 might be decreased toward, but never below, one); the latter is not, and might possibly be removed. Within these limits, calculations have been made varying the distance on the vehicle surface from the nozzle centerline to the base plane, Z_{ojet}. Results are shown in Figure 18. They are in accord with expectations.

Injector Momentum

Performance is calculated for varying values of jet velocity at fixed jet flow rate. The simplest way of doing this is by changing the injection nozzle area ratio. Results of doing so are shown in Figure 19. The decrease of base pressure with increasing jet velocity is at least consistent with the results of Schadow and Chieze,[29] although direct comparison is not possible between axisymmetric calculations and planar flow experiments.

Number of Injectors

A correction has been included in the program, almost since its earliest existence, for the failure of the individual jet flows to completely surround the base cavity.[14] It is based on limited data and on the assumption that the correction is of the form

$$\frac{P_{B_{corr}}}{P_{B_{uncorr}}} \sim \exp - \frac{\text{gap width}}{\text{base circumference}}$$

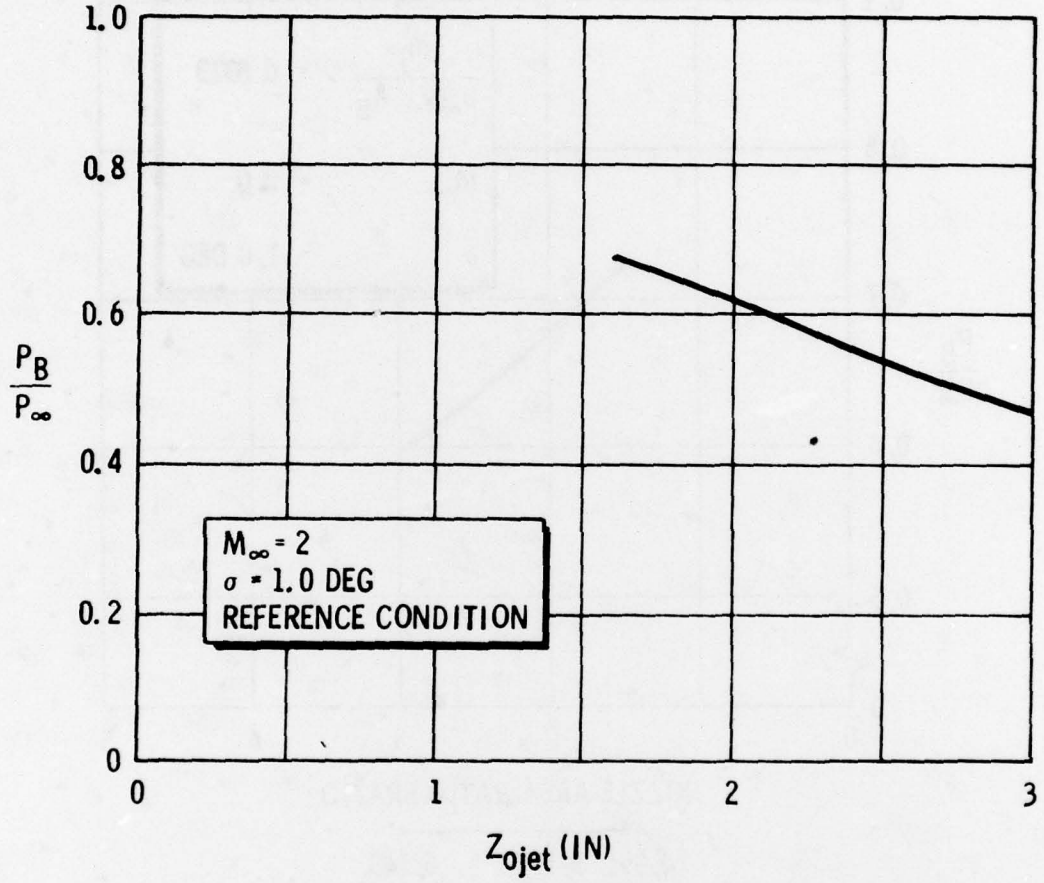

Figure 18. Effect of Injector Location

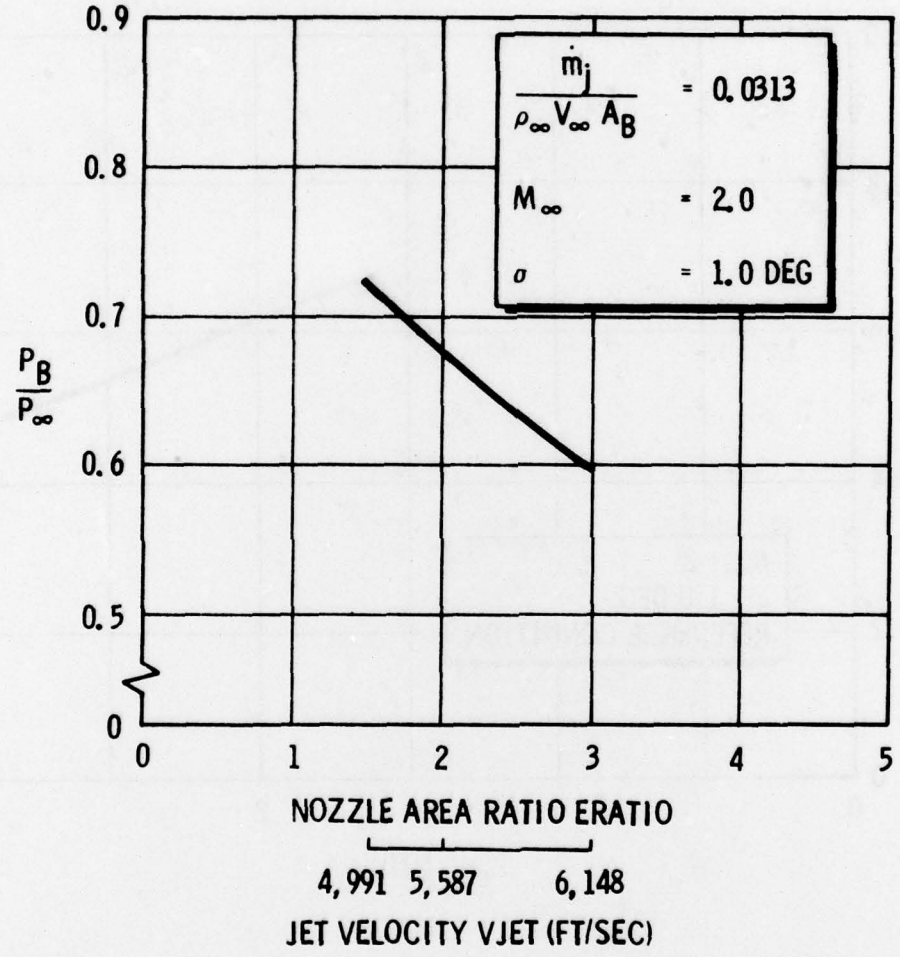

Figure 19. Effect of Injectant Momentum Flux at Fixed Mass Flowrate

where the gap width is the total length of the base perimeter that is not covered by the inner flows calculated for the individual jets, and constants multiplying the exponential function and its argument are found from the existing data points, of which there are two.[14]

In addition to this correction, there are other effects of the number of nozzles N which appear in the calculation. As N is decreased the scale of the individual jets increases with respect to the vehicle; the base plane conditions (the annulus entrance conditions) consequently change, both because the end of the turning region is shifted closer to the base plane, and because the body transverse curvature may become important (jet wraparound). These effects are shown in Figure 20. The desired range of N could not be covered because for $N < 8$ the individual-jet turning regions come too near the base. In the absence of data, the predictions shown in Figure 20 are in accord with the expectation that as N increases performance should also increase.

Other Parameters

In developing this parametric survey, emphasis was of course given to those parameters that were explicitly requested. Many other parameters are of interest and can be accounted for in the present program. Here a few of these that seem important are discussed.

Combustion Efficiency: This variable, denoted η_R or ETAR, represents the fraction of the annulus flow (or in the individual-jet calculations, of the inner flow) that is treated using chemical equilibrium. Based on the only

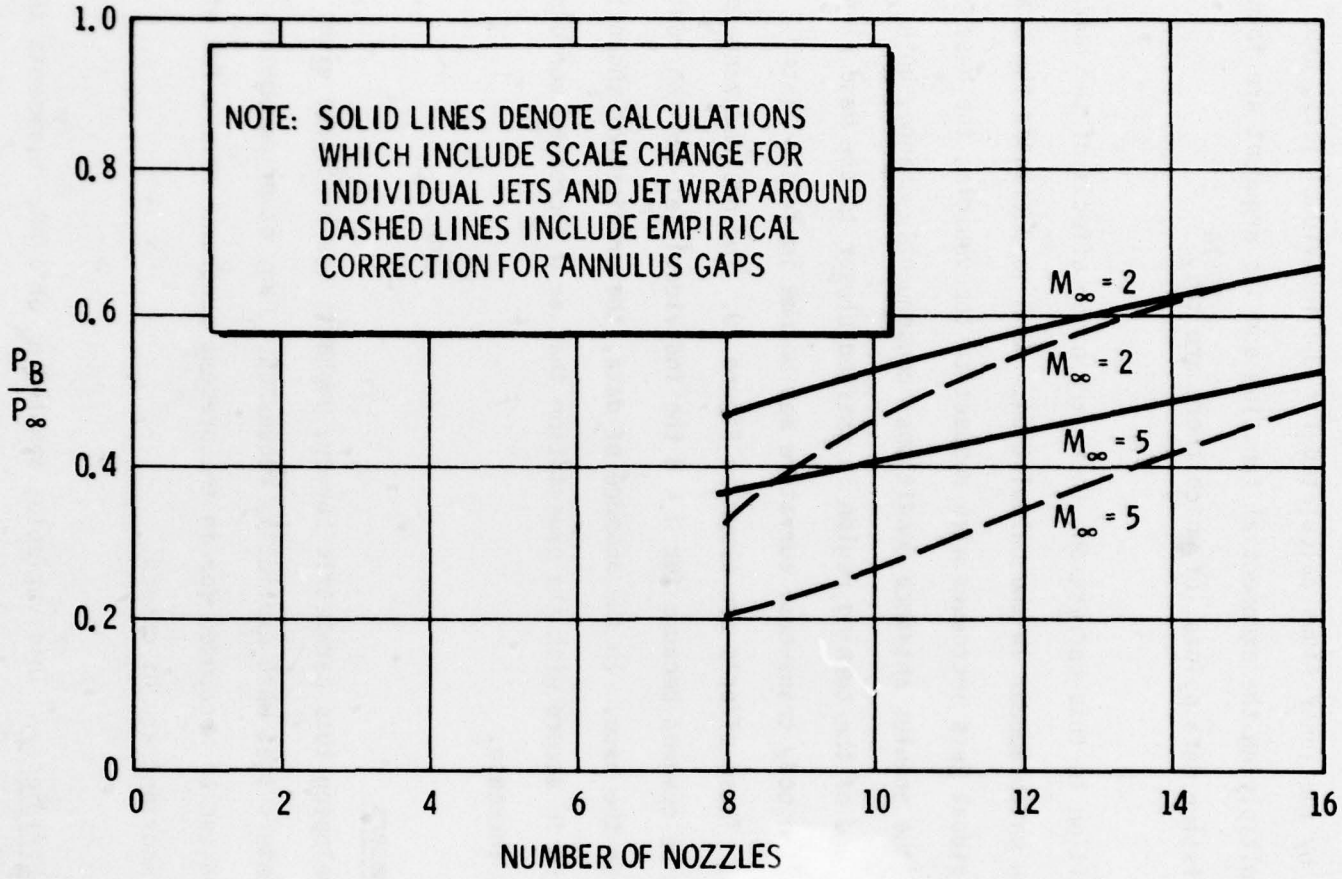

Figure 20. Effect of Number of Nozzles at Fixed Injectant Flow Rate

conclusive data on the subject,[14] the value $\eta_R = 0$ was used for all runs shown in this report. Runs for $\eta_R > 0$ can be made, and will be, in order to better understand the operation of the program.

Boattailing: It has been observed that good performance can be achieved by locating the jets on a boattail. Such a geometry can probably be approximated in the present program, though some changes, probably small, may be needed to handle a negative θ_2. The limitation to a biconic vehicle means that the body upstream of the boattail cannot be a true cylinder, and that even if θ_1 were made small, the body length would be extreme. This is not a serious problem, however, as the length has only a small effect on the inviscid flow.

Nozzle Inclination: This variable (α_{jet}) determines the distribution of overall thrust between the axial component of nozzle thrust and the rise in base pressure. As such it is a natural candidate for optimization studies. It can easily be changed in the present program, although a better understanding of the empirical-shock method may be needed to run at the lowest Mach numbers.

SECTION SIX

CONCLUSIONS AND RECOMMENDATIONS

Conclusions

The results presented above to a large extent cover the desired ranges of variables, but they do not do so completely. The main failure is in treating some injectants, although it is believed that the problems in doing so are not prohibitive. Program achievements include coverage of a range of Mach numbers that was doubtful at the beginning of the work, of two orders of magnitude in ambient pressure, and of substantial ranges of other parameters of interest. Some uncertainty is present in the results, particularly with respect to the scatter that sometimes results (e.g. Figure 15), as well as in the method chosen to eliminate multiplicity of solutions. Trends and values calculated, however, generally match data and expectations reasonably well.

Recommendations for Future Work

Although many of its results compare reasonably well with data and expectations, the model and associated code described herein fall short of what is desired in several ways. Symptoms include the inability of run with certain propellants (a difficulty which is probably not fundamental and probably can be cured with relative ease); and the more fundamental problems -- absent or multiple solutions, scatter, and the few questionable trends (e.g. the behavior of P_B/P_∞ as $P_{oj} \rightarrow 0$; the change in slope of P_B/P_∞ vs. M at $M_\infty = 2$). There are also areas where the physical representation is inadequate. The most important of these is the failure to include an inner shear layer and

the resulting viscous-inviscid interaction downstream of reattachment. Failure to explicitly satisfy the radial momentum equation is in principle equally important, although as a practical matter the error involved is in all cases observed to be relatively small (< 17%) and to probably have only a negligible effect on trends. Other physical approximations that may be of lesser importance include the assumptions of zero radial pressure gradient, of single-ray turning of the injectant annulus, of neglect of one family of characteristics in the external flow, of instantaneous transition from individual jets to an annulus at the base plane, and many others.

Of these shortcomings, two are believed most in need of additional work. These are

(1) A deeper understanding of the problem we see as multiple solutions.

(2) Inclusion of the inner shear layer and viscous-inviscid interaction.

These may be interrelated, a possibility which makes the second of higher priority. As shown in Figure 10 and the accompanying discussion, multiple solutions (which includes its alternate possibility, no solution) arise because pressures at both inner and outer boundaries of the injectant annulus are decreasing functions of θ_w, the wake cavity half-angle. Physically it is likely that the inner boundary pressure will begin to rise with increasing θ_w at large enough θ_w. This is because at very large θ_w (say near 90 deg.)

a large fraction (perhaps nearly half) of the annulus flow would be forced to recirculate; and a relatively high pressure at the cavity boundary would be required to turn inward the radially outward momentum of this flow at and near the base plane.

If the inner boundary pressure rises with increasing θ_w this guarantees a solution, subject only to the proviso that, at some smaller θ_w, $P_{inner} < P_{outer}$. This in turn changes the whole method of obtaining solutions, and in addition improves solution stability. (The latter may arise from the small-angle crossings shown in Figure 10, and may in fact be related to the scatter in some of the program predictions that is referred to above.) The interrelation comes from the fact that item (2) above, the inclusion of the inner shear layer and the interaction of its viscous wake with the approximately inviscid annulus and external flows, is required in order to see this increase of P_{inner} with θ_w that is expected on physical grounds.

Although the work described above should probably be given priority, other work is also recommended, though probably at a lower level of importance. Several other assumptions have been mentioned above, and they are not a complete list. The inaccuracies resulting are probably smaller but not negligible. It is recommended that estimates be made of the magnitude of the inaccuracy generated by at least the apparently most important of these assumptions (including those judged more important, as above). When this is done, an informed assessment both of the expected program accuracy and the best subject for further work can be made.

NOMENCLATURE

A	Area
A_B	Vehicle base area
A	Injectant nozzle throat area
h	Jet scale length ("penetration height"); altitude
M_L	Local Mach number
M_∞	Flight Mach number
$\dot{m}$	Mass flowrate
$\dot{m}_j$	Injectant mass flowrate (If no units are specified, units are $\rho_\infty V_\infty A_B$)
N	Number of nozzles
P	Pressure
R	Radius
v	Velocity
x_{BODY}	Length of vehicle
x_{CONE}	Length of vehicle nose cone

α	Angle of equivalent single ray
α_i	Inclination of jet with respect to normal to centerline; positive upstream
γ	Ratio of specific heats
δ	Annulus divergence angle
$\delta\dot{m}_d$	Mass entrained downstream of expansion ray
$\delta\dot{m}_u$	Mass entrained upstream of expansion ray
η_R	Reaction efficiency (fraction of flow at equilibrium; remainder frozen)
θ	Turning angle
θ_1	First cone half-angle of biconic vehicle
θ_2	Second cone half-angle of biconic vehicle
θ_c	Second cone half-angle of biconic vehicle ($\equiv\theta_2$)
θ_w	Cavity half-angle
μ	Mach angle
ν	Prandtl-Meyer angle
ρ	Density
σ	Mixing half-angle

SUBSCRIPTS

i	Annulus leading edge
i+1	Annulus trailing edge
in	Annulus inner boundary
out u	Annulus outer boundary, upstream of expansion ray
out d	Annulus outer boundary, downstream of expansion ray
1	External flow at annulus leading edge
2	External flow immediately after expansion ray
0	Stagnation values

REFERENCES

1. Warren C. Strahle, "Theoretical Consideration of Combusion Effects on Base Pressure in Supersonic Flight," Twelfth Symposium (International) on Combustion, The Combustion Institute, Pittsburgh, Pa., 1969.

2. J. E. Bowman and W. A. Clayden, "Cylindrical Afterbodies in Supersonic Flow with Gas Injection," AIAA Journal, Vol. 5, No. 8, August 1967; pp. 1524-1525.

3. G. A. Hosack and R. A. O'Leary, "Base Burning Feasibility Investigation, Volume I - Technical Report (U)," Rocketdyne Report No. RK-TR-70-17, December 1970 (classified Confidential).

4. H. L. Fein and R. J. Cavalleri, "An Investigation of External Burning Propulsion for Missile Applications," Atlantic Research Corp. Report AFRPL-TR-75-43, March 1976.

5. I. E. Alber and L. Lees, "Integral Theory for Supersonic Turbulent Base Flows," AIAA Journal, Vol. 6, July 1968, pp. 1343-1351.

6. H. H. Tang and D. S. Chaussee, "Analysis of Base Burning Methods and Applications," AIAA Progress in Astronautics and Aeronautics: Aerodynamics of Base Combustion, Vol. 40, edited by Murthy, Osborn, Barrows, and Ward, New York, 1976, pp. 349-383.

7. J. A. Schetz, F. S. Billig, and S. Favin, "Simplified Analysis of Supersonic Base Flows Including Injection and Combustion," AIAA Journal, Vol. 14, January 1976, pp. 7-8.

8. J. A. Schetz, S. Favin, and F. S. Billig, "Analytical Comparison of the Performance of Different Base Burning Modes," AIAA Journal, Vol. 14, September 1976, pp. 1337-1338.

9. D. W. Harvey, B. R. Phillips, D. F. Hopkins, and I. Catton, "A Model of External Burning of Liquid Fuels," AIAA Journal, Vol. 15, March 1977, pp. 309-313.

10. D. W. Harvey and I. Catton, "A Model of Base Burning Propulsion Using Lateral Injection," AIAA Journal, Vol. 15, September 1977, pp. 1372-1373.

11. D. W. Harvey, D. F. Hopkins, W. A. Gaubatz, J. M. Kallis and R. Rosen, "Combined Endo-Exoatmospheric Reaction Control System, Volume I: Analysis, Computer Program, Systems Application and Follow-on Programs (U)," McDonnell Douglas Report MDC G0629-I, October 1970 (classified Confidential).

12. D. W. Harvey, D. F. Hopkins, J. M. Kallis and C. R. Easton, "Specific Impulse Prediction for Reactive Jet Interaction (U)," McDonnell Douglas Paper WD-1516, April 1971; presented to the AIAA 7th Propulsion Joint Specialist Conference, Salt Lake City, Utah, June 1971 (classified Confidential).

13. D. W. Harvey and D. F. Hopkins, "Fluid Mechanics of Jet Interaction and External Burning Controls (U)," McDonnell Douglas Report MDC G6174, January 1976 (classified Confidential).

14. D. W. Harvey and D. F. Hopkins, "Advanced Interceptor Control and Base Burning Technology Study, Vol. II: External Burning Propulsion (U)," McDonnell Douglas Report MDC G7341, February 1978 (classified Confidential).

15. D. R. Chapman, "An Analysis of Base Pressure at Supersonic Velocities and Comparison with Experiment," NACA Report 1051, 1951.

16. J. M. Kallis, "Equivalent Solid Obstacle for Gas Injection into a Supersonic Stream," AIAA Journal, Vol. 10, October 1972, pp. 1342-1344.

17. S. H. Maslen, "Inviscid Hypersonic Flow Past Smooth Symmetric Bodies", AIAA Journal, Vol. 2, June 1964, pp. 1055-1061.

18. S. K. Jackson, "The Viscous-Inviscid Hypersonic Flow of a Perfect Gas Over Smooth Symmetric Bodies", PhD Thesis, University of Colorado, Boulder, Colorado, 1966.

19. D. W. Harvey, D. F. Hopkins, and R. Rosen, "Experiments on Reacting Gas Jet Penetration," AIAA Journal, Vol. 15, January 1977, pp. 76-82.

20. D. W. Harvey, "A Simple Scale Length for Shocks about Transverse Gas Jets," J. Spacecraft & Rockets, Vol. 14, April 1977, pp. 252-253.

21. F. S. Billig, "Shock-wave Shapes Around Spherical and Cylindrical Nosed Bodies," J. Spacecraft and Rockets , Vol. 4, June 1967, pp. 822-823.

22. H. W. Liepmann and A. Roshko, "Elements of Gasdynamics," Wiley, New York, 1957.

23. W. H. Webb, "An Approximate Pressure-Angle Relation for the Axisymmetric Supersonic Near Wake," AIAA Journal, Vol. 6, July 1968, pp. 1427-1428.

24. G. K. Mehta and W. C. Strahle, "A Theory of the Supersonic Turbulent Axisymmetric Near Wake Behind Bluff-Base Bodies", AIAA Journal, Vol. 15, August 1977, pp. 1059-1060.

25. G. L. Brown and A. Roshko, "On Density Effects and Large Structure in Turbulent Mixing Layers," Journal of Fluid-Mechanics, Vol. 64, 1974, pp. 775-816.

26. S. F. Birch, D. H. Rudy and D. M. Bushnell (eds.), "Free Turbulent Shear Flows, Vol. I - Conference Proceedings," NASA SP-321, 1972.

27. Y. H. Oh, "Calculation of Compressible Turbulent Free Shear Layers," AIAA Journal, Vol. 12, 1974, p. 401.

28. F. Baltakis, private communication, October 1976.

29. K. C. Schadow and D. S. Chieze, "External Burning Injection Study," Report AFRPL-TR-78-25, Naval Weapons Center, China Lake, California, April 1978.